Biological Journal of the Linnean Society, 2018, **XX**, 1–22. With 6 figures.

Neurocranium shape variation of piranhas and pacus (Characiformes: Serrasalmidae) in association with ecology and phylogeny

KELLY S. BOYLE* and ANTHONY HERREL

UMR 7179 C.N.R.S./M.N.H.N., Département d'Ecologie et de Gestion de la Biodiversité, 57 rue Cuvier, Case postale 55, Paris Cedex 5 75231, France

Received 19 March 2018; revised 14 June 2018; accepted for publication 15 June 2018

The teleost neurocranium houses the brain and sense organs, articulates with the upper jaw and suspensorium, and provides the attachment site for muscles involved in feeding, ventilation and locomotion. Serrasalmid fishes (piranhas and pacus) exhibit variation in diet, body shape and habitat that all may influence the evolution of neurocranium shape. In addition, serrasalmids are otophysans with well-developed hearing provided by modified ears and anterior vertebrae that may also influence otic neurocranium morphology. We conducted a 3D geometric morphometrics analysis on high-resolution tomographic data (micro-computed tomography) from 54 museum specimens to measure neurocranium shape variation and disparity among 20 species from the three major serrasalmid clades. We found broad shape variation among species that was explained by phylogenetic history and ecology and related to features such as orbit size and skull depth. Pterotic spine length was longest in carnivorous piranhas and impacts the anatomy of the adductor musculature involved in biting. We found evidence that the otic neurocranium is a separate evolutionary module influenced by both phylogeny and ecology. Lagenar bulla size and position differed among ecological groups and thus sound may vary in importance among species. Small bullae were found in rheophilic herbivores that live among noisy rapids. Thus, serrasalmid neurocranium shape may vary with the relative size of sense organs and with functional aspects of feeding and prey handling.

ADDITIONAL KEYWORDS: basioccipital – comparative analyses – exoccipital – Otophysi – parasphenoid – prootic – prootic foramen – Weberian apparatus.

INTRODUCTION

The neurocranium is an important structure in vertebrates that encloses the brain, houses sensory organs, and provides insertion sites for muscles involved in feeding, ventilation and locomotion (Hanken & Hall, 1993; Hanken & Thorogood, 1993; Helfman *et al.*, 2009). The neurocranium consists of the chondrocranium, formed from cartilaginous capsules that develop around the sense organs of the head, and the dermatocranium, which consists of superficial bones thought to have evolved from scales (Helfman *et al.*, 2009). Teleost fishes exhibit a broad diversity in neurocranium morphology (Gregory, 1933; Alexander, 1964; Arratia, 2003). In addition to phylogenetic patterns, head and neurocranium shape are predicted to be associated with variation in sensory function, feeding adaptations and locomotion (Alexander, 1964; Clabaut *et al.*, 2007; Helfman *et al.*, 2009; Schmitz & Wainwright, 2011b).

Because the neurocranium supports major sensory organs, a strong relationship between morphology associated with sense organs and ecological features of taxa, such as habitat characteristics and prey type, may be predicted. For example, nocturnal fishes are thought to have larger eye diameters to increase sensitivity to low-light conditions for feeding at night (Goatley & Bellwood, 2009; Schmitz & Wainwright, 2011a). Thus, variation in the relative importance of olfaction, vision, hearing, balance and lateral line organs may influence the morphological evolution of the neurocranium. In addition, size-related changes in processing regions of the brain may further influence

*Corresponding author. E-mail: kellyboyle.info@gmail.com

Downloaded from https://academic.oup.com/biolinnean/advance-article-abstract/doi/10.1093/biolinnean/bly092/5057832
by Natural History Museum user
on 24 July 2018

the relative size and shape of the cranium (Striedter & Northcutt, 2006).

For aquatic animals, the shape of the cranium may be especially important for locomotion because of the density of the surrounding medium and the drag forces experienced during locomotion (Segall *et al.*, 2016). There may be a relative trade-off between drag and the relative depth of the head and the ability to manoeuvre and make rapid turns (Webb, 1984, 2005). Furthermore, the shape of the head is related to overall body depth (Alexander, 1964), a feature that may reduce the number of potential predators by gape limitation (Nilsson & Brönmark, 2000; Claverie & Wainwright, 2014).

Neurocranium shape can be expected to be influenced by functional demands influencing the evolution of muscles involved in locomotion, feeding and ventilation. For example, the supraoccipital forms the anterior origin of the epaxial musculature of the body (Alexander, 1964; Winterbottom, 1974). Moreover, some adductor mandibulae fibres, involved in closing the lower jaw and biting, originate on portions of the neurocranium (Alexander, 1964; Winterbottom, 1974; Datovo & Castro, 2012). Thus, neurocranium shape variation may influence the size and position of the origins of cranial muscles, which would be expected to have functional consequences. In addition, neurocranium shape variation influences the position of other cranial bones, which could influence the position and size of cranial muscles and the biomechanics of feeding and ventilation. For example, neurocranium shape influences the position of the suspensorium that articulates with the lower jaw, position of the upper jaw, opercular series and gill arches.

The shape of the otic region of the neurocranium can be expected to be related to the function of the ears in hearing and balance. Changes in size and shape of otic bones may be associated with size differences of the semicircular canals and otolithic end organs of the ear. The relative sizes of otoliths and sensory maculae vary substantially in fishes (Popper & Fay, 2011). Among otophysan fishes, the relative sizes of the asteriscsus otolith and associated lagenar end organ are substantially larger than in most teleosts, while the sagitta and saccule are relatively reduced in size (Popper & Fay, 2011). The lagenar otoliths lie within large lateral capsules of the neurocranium in otophysans (Frost, 1925). The lagena of otophysan fishes is thought to be involved in the detection of sound particle motion, while the sacculus functions principally in the role of indirect detection of sound pressure stimuli that are transduced by the Weberian apparatus (Fay, 1984; Popper & Fay, 2011). The Weberian apparatus morphology (Weber, 1820) is unique to otophysan fishes and involves a chain of ossicles connected by ligaments and associated with the anterior vertebrae. This morphology is associated with additional modifications of the otic region of the skull, in which a medial opening, the cavum sinus impar, exists ventral to the foramen magnum. Sound pressure-induced vibrations of the swim bladder are mechanically transduced to the anterior Weberian ossicles (scaphiae). The cavum sinus impar allows fluid motion between the scaphiae and a perilymphatic space (sinus impar) in the inner ears of otophysan fishes (Alexander, 1962; Popper & Fay, 1973; Chardon & Vandewalle, 1997). As a result of this morphology, otophysan fishes are able to hear higher frequencies of sound pressure in comparison to most other teleosts (von Frisch, 1938; Popper, 1972; Ladich, 1999; Yan *et al.*, 2000; Mélotte *et al.*, 2018).

Serrasalmid fishes (piranhas and pacus) provide an opportunity to examine variation of the neurocranium among species that vary in feeding ecology, feeding behaviour and phylogenetic history. This characiform family is composed of approximately 93 species (Eschmeyer & Fong, 2017) and 16 extant genera (Thompson *et al.*, 2014) with a broad distribution in South America from Atlantic coast river drainages to the eastern slopes of the Andes. The family includes fruit-eating and seed-dispersing species (Goulding, 1980; Goulding & Carvalho, 1982; Horn *et al.*, 2011) and carnivorous species with diets that vary in relative importance and include whole prey of invertebrates and fishes and pieces of larger fishes (fins and scales) (Machado-Allison & Garcia, 1986; Nico & Taphorn, 1988; Sazima & Machado, 1990; Nico, 1991). Several rheophilic herbivore species of serrasalmids are restricted to high-energy river environments with torrents and rapids and feed extensively on submerged aquatic plants of the family Podostemaceae (Jégu & Dos Santos, 2002; Jégu *et al.*, 2002a, b; Jégu & Keith, 2005; Andrade *et al.*, 2013). In addition, serrasalmid body shapes range from moderately slender to relatively deep-bodied. Thus, the neurocranial morphology of serrasalmid species may be influenced by a variety of factors: phylogenetic history, feeding morphology, body shape and sensory morphology. Variation in habitat and feeding behaviour may require a larger role of certain sensory modalities, such as vision and hearing. For example, there is anecdotal evidence that splash sounds associated with falling seeds and fruits may be attractive to some fruit-eating serrasalmids (Gottsberger, 1978; Piedade *et al.*, 2006; Correa *et al.*, 2007; Parolin *et al.*, 2010) and carnivorous piranhas are reported to be attracted to splashing sounds from wounded prey and the feeding activities of other piranhas (Markl, 1972; Stabentheiner, 1988; Mol, 2006). In contrast, rheophilic herbivorous serrasalmids probably live in a noisier environment and their diet of submerged aquatic plants may not be associated with an acoustic stimulus.

Downloaded from https://academic.oup.com/biolinnean/advance-article-abstract/doi/10.1093/biolinnean/bly092/5057832
by Natural History Museum user
on 24 July 2018

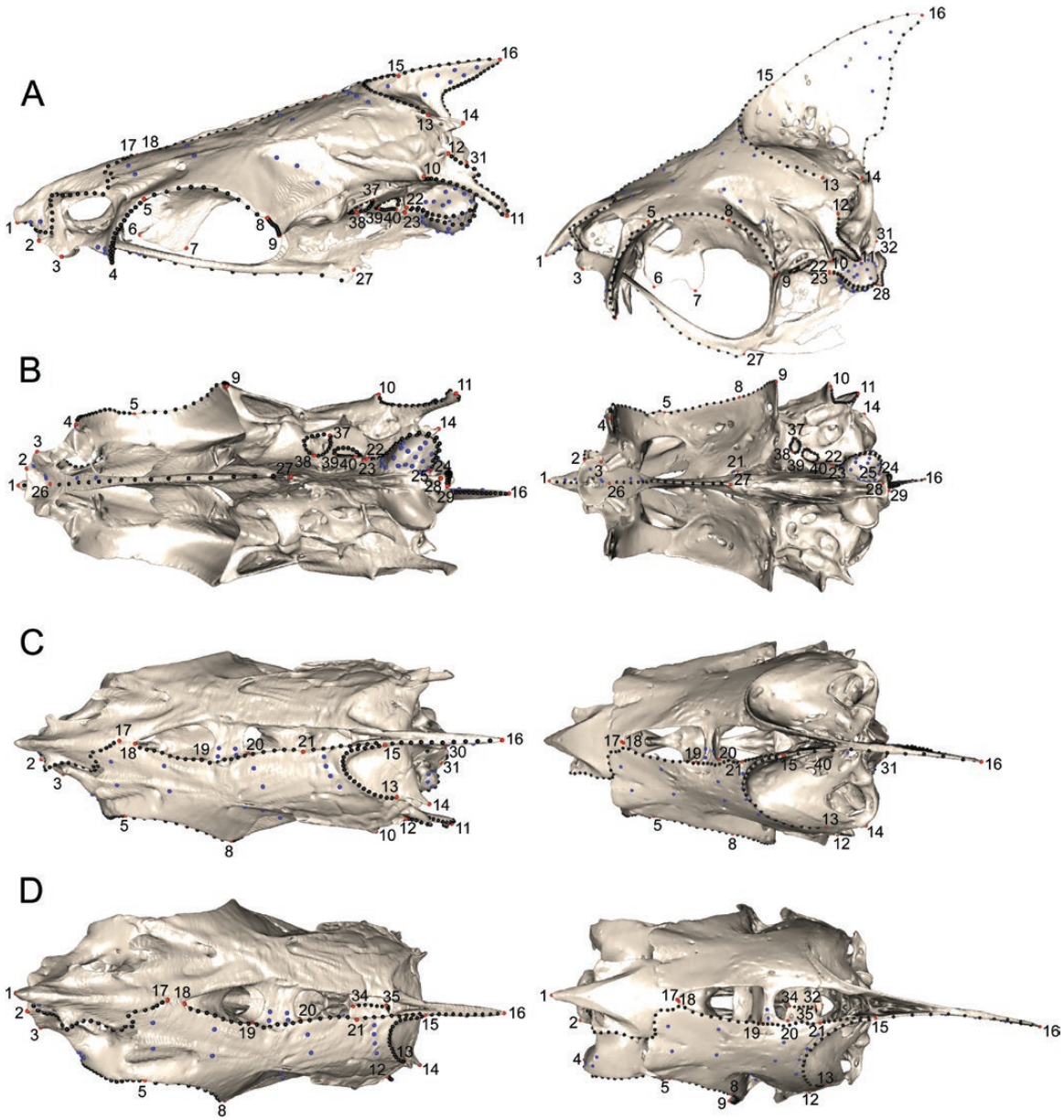

Figure 1. Landmarks used in analyses to quantify shape variation of the left side of the neurocranium. Reconstructions come from *Serrasalmus elongatus* Kner, 1858 MNHN IC.1989.1360 (left in each pane) and *Myleus setiger* (Müller & Troschel, 1844) MNHN IC.1998.1156 (right). A, lateral view; B, ventral view; C, dorsal view; D, oblique dorsal anterior view. Numbered red dots correspond to landmarks (see Table 1 for definitions). Black dots represent sliding semi-landmarks on curves. Blue dots represent sliding surface landmarks.

Serrasalmid neurocranium morphology is predicted to be influenced by both phylogenetic history and ecology. In addition, feeding ecology in serrasalmids is influenced by phylogenetic history (K. S. Boyle & A. Herrel, unpubl. obs.). We tested five hypotheses. (1) Neurocranium morphology is associated with phylogeny and (2) neurocranium morphology is partly explained by ecology, even after accounting for phylogenetic history. In addition, because hearing may be especially relevant to the ecology of otophysan fishes, and because we predict different sound cues to be relevant to specific serrasalmid feeding ecologies, we expected a relationship between ecology and otic neurocranium morphology. We tested hypothesis (3) that the otic neurocranium has evolved as a modular structure relative to the rest of the neurocranium, (4) that otic neurocranium morphology is associated with phylogeny and (5) that otic neurocranium morphology is partly explained by ecology after

Downloaded from https://academic.oup.com/biolinnean/advance-article-abstract/doi/10.1093/biolinnean/bly092/5057832
by Natural History Museum user
on 24 July 2018

accounting for phylogenetic history. We tested for allometry as an alternative explanation of shape variation of the neurocranium and otic neurocranium. We also examined areas of pattern-based morphological convergence of species within and among ecological groups that may explain neurocranium morphological variation among serrasalmids. In addition, we tested for differences in disparity among ecological groups and among the three major clades: piranha, *Myleus*-pacus and pacu (*sensu* Ortí *et al.*, 2008; Thompson *et al.*, 2014).

MATERIAL AND METHODS

PHYLOGENY

A composite phylogeny (Supporting Information, Fig. S1) was constructed based on data from molecular phylogenies (Ortí *et al.*, 2008; Thompson *et al.*, 2014; Andrade *et al.*, 2017) that together included 18 of the 20 species in our study. Our study included two species that were not present in available phylogenetic hypotheses: *Metynnis lippincottianus* (Cope, 1870) and *Serrasalmus elongatus* Kner, 1858. We inferred the phylogenetic position of these two taxa based on taxonomy and placed *M. lippincottianus* as sister to its only congener in our dataset, *M. hypsauchen* (Müller & Troschel, 1844), and we placed *S. elongatus* as sister to *S. rhombeus* (Linnaeus, 1766) in a nexus file made based on the Thompson *et al.* (2014) phylogeny. To construct the composite phylogeny, we used the matrix with rate parsimony (mrp) method (Sanderson *et al.*, 1998). Phylogeny nexus files were transformed into a 'multiphylo' object with the 'c.phylo' function of the 'APE' library (Paradis *et al.*, 2004) in R (R Core Team, 2017). The composite tree was produced using the 'pratchet' method and 10 000 iterations using the 'mrp.supertree' function of 'phytools' R library (Revell, 2017). We used branch length estimates from Thompson *et al.* (2014) when available. When branch length estimates were not available, we assigned branch length values by evenly dividing evolutionary time of the most recent calibrated node among the remaining branches (Aquino & Colli, 2017).

SPECIMENS, µCT SCANS AND 3D RECONSTRUCTIONS

Specimens from the study were obtained from the Ichthyology Collection at the Muséum National d'Histoire Naturelle (MNHN), Paris, France (Table S1). We used micro-computed tomography (µCT) scanning to produce 3D surfaces of the neurocranium (Figs 1, 2). Specimens were scanned at the AST-RX technical platform at the MNHN with a µCT scanner (v|tome|x 240 L, GE Sensing & Inspection Technologies phoenix|x-ray). Voxel sizes ranged from 31.1 to 100.0 µm (mean 53.6). Segmentation and

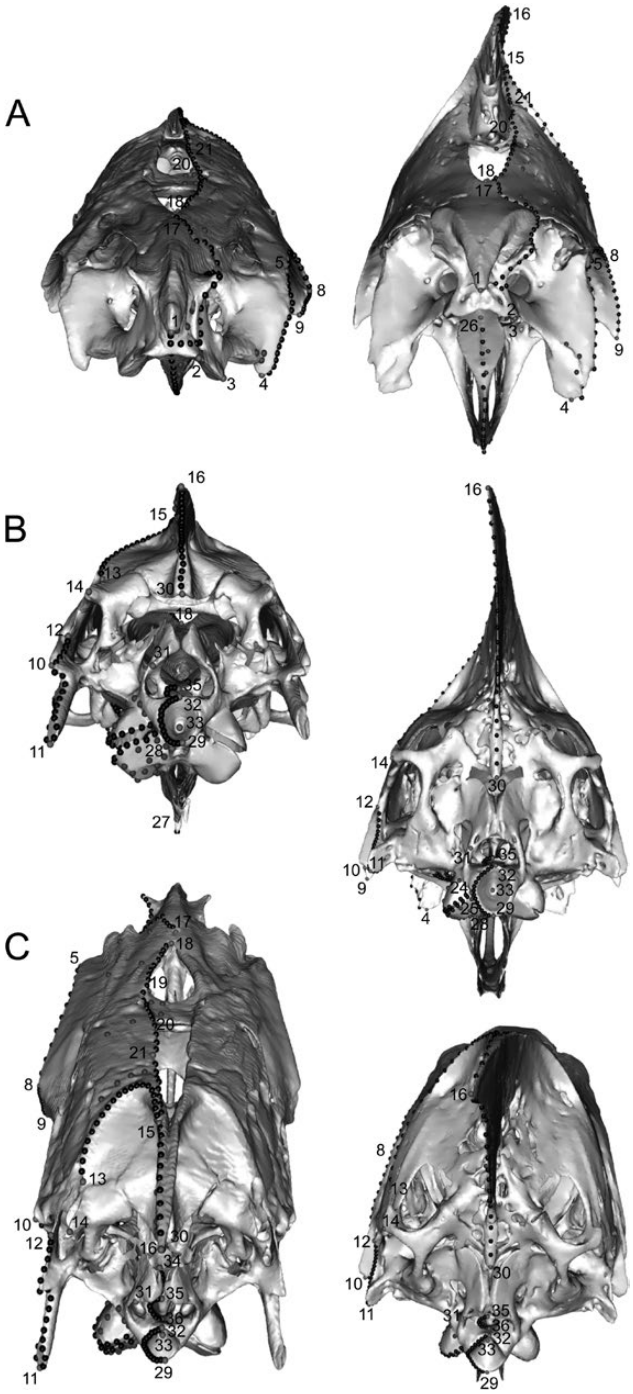

Figure 2. Landmarks used in analyses to quantify shape variation of the left side of the neurocranium. Reconstructions come from *Serrasalmus elongatus* MNHN IC.1989.1360 (left in each pane) and *Myleus setiger* MNHN IC.1998.1156 (right). A, anterior view; B, posterior view; C, oblique dorsal posterior view. Numbered red dots correspond to landmarks (see Table 1 for definitions). Black dots represent sliding semi-landmarks on curves. Blue dots represent sliding surface landmarks.

Downloaded from https://academic.oup.com/biolinnean/advance-article-abstract/doi/10.1093/biolinnean/bly092/5057832
by Natural History Museum user
on 24 July 2018

Table 1. 3D geometric morphometric homologous landmark definitions

Landmark	Definition
1	Anterior tip of mesethmoid
2	Anteriolateral corner of vomer
3	Posteriolateral corner of vomer
4	Ventral tip of the lateral ethmoid
5	Suture of lateral ethmoid and frontal along lateral edge
6	Anterior or superior corner of the orbitosphenoid (depends on orientation of bone in different specimens)
7	Posterior or inferior corner of the orbitosphenoid (depends on orientation of bone in different specimens)
8	Suture of frontal and sphenotic, along lateral edge
9	Ventral tip of sphenotic
10	Inferior corner of pterotic spine
11	Tip of pterotic spine
12	Superior corner of pterotic spine
13	Intersection of the parietal, supraoccipital and epioccipital at the posterior margin of the parietal
14	Tip of the epioccipital
15	Suture between parietal and supraoccipital along the dorsal ridge
16	Tip of supraoccipital crest
17	Centre of mesethmoid, posteriorend
18	Anterior medial corner of frontal bone along the frontal fonatenelle
19	Left, anterior intersection of epiphyseal bar and frontal
20	Left, posterior intersection of epiphyseal bar and frontal
21	Suture between the parietal and frontal along the frontal fontanelle
*22	Anterior ventral corner of exoccipital, just superior to the basioccipital
*23	Anterior dorsal corner of basioccipital, just inferior to the exoccipital
*24	Posterior edge of the lagenar bulla and exoccipital
*25	Posterior edge of the lagenar bulla and basioccipital
26	Junction of anterior end of parasphenoid and vomer
27	Ventral tip of the parasphenoid, below orbit, crux below the posterior margin of the orbit, anterior to the lamellae that fuse to the basioccipital
28	Posterior end of left basioccipital lamellae
*29	Ventral medial point of vertebral articulation on basioccipital
30	Posterioventral tip of supraoccipital
31	Anterior portion of exoccipital that meets a strut along the edge of the foramen magnum
32	Dorsal medial point of vertebral articulation on basioccipital
*33	Centre of vertebral articulation on basioccipital
*34	The medial edge of the anterior end of the left exoccipital bone that lies over the sinus endolymphaticus
*35	The medial edge of the posterior portion of the exoccipital, superior to the sinus impar
*36	The medial point of the posterior opening of the cavum sinus impar, part of exoccipital
*37	Lateral corner of nVII foramen in prootic
*38	Medial corner of nVII foramen in prootic
*39	Anterior corner of the prootic 'auditory' foramen
*40	Posterior corner of the prootic 'auditory' foramen

*Landmarks used in the subset of data of the auditory neurocranium.

surface generation were performed using AVIZO 7.0 (FEI, Mérignac, France). Semi-automatic thresholding was used to identify bone. A drawing tablet was used to manually isolate the bones of the neurocranium from the other bones of the skull, the supraneural of the neural complex, first vertebra, scaphium, posttemporal bones and the otoliths. The remaining segmented bones were used to create a singular bilateral neurocranium surface file that consisted of the vomer, mesethmoid, lateral ethmoids, frontals, parasphenoid, orbitosphenoid, parietals, occipitals, supraoccipitals, sphenotics, pterotics, prootics, basioccipital, exoccipitals and intercalars. Surface generation was performed using the 'constrained smoothing' setting in AVIZO 7.0. Surfaces were exported as (.PLY) format files. Surface files were decimated to reduce file size (between 440 176 and 1 607 463 triangles) and cleaned to fill-in holes, remove creased edges remove and spikes with

Downloaded from https://academic.oup.com/biolinnean/advance-article-abstract/doi/10.1093/biolinnean/bly092/5057832
by Natural History Museum user
on 24 July 2018

Geomagic Studio software (Geomagic Studio; Raindrop Geomagic, Research Triangle Park, NC, USA). We analysed shapes of the left side of the neurocranium (left elements of paired bones and the left portion from the midline of unpaired elements). Several specimens (Table S1) had irregularities on the left side in which the auditory foramen, nVII foramen or both were not fully ossified and were open to the margin of the prootic and one specimen had a damaged left lagenar bulla. These specimens were mirrored in Geomagic Studio and the right side was used for analysis.

Ecological groups

Fish species were categorized into three broad ecological groups for analysis based on published accounts of feeding habits and habitat associations (Table S1). These ecological groups were: (1) carnivores, species that mainly consume fish prey either whole or in pieces (muscle tissue, lepidophagy, fins); (2) frugivores/granivores, species that consume a substantial portion of fruits and seeds; and (3) rheophilic herbivores, species that are restricted in habitat to high-flow environments among rapids and waterfalls and that have a largely herbivorous diet composed of submerged plants. We distinguished rheophilic herbivores from herbivorous and omnivorous frugivore/granivore species because these species are more restricted in habitat to high-energy environments and feed mainly on submerged associated plants associated with these habitats, such as species in the family Podostemaceae (Jégu *et al.*, 2002a, b; Jégu & Keith, 2005; Dary *et al.*, 2017). Other serrasalmid species in our study can occur among rapids (e.g. Fitzgerald *et al.*, 2018), but have broader habitat associations and differ in feeding ecology (Table S1). *Acnodon normani* Gosline, 1951, a Brazilian shield species with a broad diet that includes fruits, seeds, leaves, insects and scales (Leite & Jégu, 1990), was included in the frugivore/granivore group. This species tends to occur in slow to moderate flowing waters, relative to more rheophilic serrasalmids (Zuanon, 1999). Ancestral state reconstruction indicates that a frugivore/granivore ecology is the ancestral condition for the species in our dataset (K. S. Boyle & A. Herrel, unpubl. obs.) and occurs in 11 of 20 species in our study, including all members of the pacu clade, most members of the *Myleus*-pacu clade, and within the genus *Metynnis* of the piranha clade. Ancestral state reconstruction indicats that rheophilic herbivory, which in our dataset occurs as a monophyletic lineage with the *Myleus*-pacu clade, probably evolved once (K. S. Boyle & A. Herrel, unpubl. obs.). Carnivores occur as a derived monophyletic clade within the piranha clade and probably evolved once (K. S. Boyle & A. Herrel, unpubl. obs.).

Geometric morphometric landmarks

Forty homologous landmarks (Table 1) were identified and placed on the left (l.) side of the neurocranium (Fig. 2). Homologous landmarks were placed on the mesethmoid, vomer, l. lateral ethmoid, l. frontal, l. orbitosphenoid, l. sphenotic, l. pterotic, l. parietal, supraoccipital, l. epioccipital, epiphyseal bar, l. exoccipital, basioccipital and parasphenoid of surface files in IDAV Landmark software (Wiley *et al.*, 2005). We used a combination of traditional homologous landmarks and sliding 3D semi-landmarks with the goal of providing a better description of structures devoid of good homologous landmarks (Bookstein, 1997; Gunz *et al.*, 2005). Sliding semi-landmarks are geometrically homologous landmarks that can be used to increase the resolution to describe shapes (383 landmarks in total). Curve semi-landmarks were allowed to slide along a trajectory between defined homologous landmarks and surface semi-landmarks were allowed to slide across surfaces. Curve semi-landmarks were placed along curve features between homologous landmarks using the Landmark software. A total of 21 curves with 8–20 semi-landmarks per curve was used (280 semi-landmarks in total). Curves were placed along the left side of the frontal fontanelle from the supraoccipital crest; to the anterior end of the fontanelle; around the left margin of the mesethmoid; along the ventral midline of the parasphenoid; along the left margin of the orbit; around the left pterotic spine; along the caudal midline of the supraoccipital; along the curve between the supraoccipital, parietal and epioccipital on the left side; and around the left side of the basiocciptal at its articulation with vertebra 1 (Fig. 1). In addition, several curves associated with the otic region of the neurocranium were chosen (Fig. 1): a curve along the ventral margin of the exoccipital along the dorsal portion of the left lagenar bulla; a curve along the dorsal margin of the basioccipital along the ventral portion of the left lagenar bulla; a curve around the left side to the midline of the posterior opening of the cavum sinus impar; a curve along the left-medial edge of the dorsal surface of exoccipital bone within the brain case that covers the sinus endolymphaticus of the ears; a curve around a foramen in the prootic for a ramus of nVII that is open to the utricle; and a curve around the prootic foramen, a characiform synapomorphy (Fink & Fink, 1981) that is also open to the utricle. To generate semi-landmarks, a single specimen for each bone was arbitrarily chosen as an initial template. Surface landmarks were added to the template using Landmark software and used to project surface landmarks on to all the specimens for each bone or otolith using the 'placePatch' function of the 'Morpho' library (Schlager, 2015) in R (R Core Team, 2017). Eleven surface landmarks were placed on the l. exoccipital over the dorsal,

Downloaded from https://academic.oup.com/biolinnean/advance-article-abstract/doi/10.1093/biolinnean/bly092/5057832
by Natural History Museum user
on 24 July 2018

outer portion of the lagenar bulla, 18 on the basioccipital on the lower outer portion of the left lagenar bulla, seven on the left side of the supraoccipital crest, three on the dorsal surface of the l. sphenotic, six on the dorsal surface of the l. frontal, two on the parasphenoid, three on the vomer, three on the l. lateral ethmoid, two on the mesethmoid and four on the left side of the ephiphyseal bar. Curve and semi-landmarks were slid using 'Morpho' (Schlager, 2015) to minimize the bending energy of the thin plate spline, first between each specimen and the template (over five iterations), and then between each specimen and the Procrustes consensus of the entire dataset over ten iterations (Gunz *et al.*, 2005; Botton-Divet *et al.*, 2015).

Subsequent analyses were done on the full left neurocranium 383 landmark dataset as well as a subset of landmarks that characterizes the otic region of the skull. This subset included ten of the original homologous landmarks (Table 1) from the sliding procedure described above, and the curves on the exoccipital and basioccipital over the lagenar bulla, the curves around the nVII foramen and prootic foramen, the curve over the dorsal roof of the sinus endolymphaticus, the curve around the left side of the exoccipital's articulation with vertebra 1, and the curve around the left side of the cavum sinus impar. This subset of landmarks included the surface landmarks of the dorsal and ventral portions of the left lagenar bulla. This subset of otic neurocranium data included a total of 320 landmarks (landmarks, curve semi-landmarks and surface landmarks).

Generalized Procrustes superimpositions (Rohlf & Slice, 1990) of the entire data set and for the auditory neurocranium subset were conducted in the 'geomorph' library (Adams *et al.*, 2016) in R (R Core Team, 2017) using the 'gpagen' function. For this Procrustes superimposition, the previously slid curve and surface semi-landmarks were treated as fixed landmarks. For each dataset, the mean shape of each species was calculated using the 'mshape' function of 'geomorph' in order to allow for phylogenetic comparisons among species. A second Procrustes superimposition on the species means was then calculated for each structure as described above using the 'gpagen' function of 'geomorph' for subsequent analyses. Principal components analysis (PCA) was conducted on the species means using 'PlotTangentSpace' in 'geomorph'. Phylogenetic relationships with the PCA morphospace were visualized with the 'phylomorphospace' function in the 'phytools' library (Revell, 2017) in R (R Core Team, 2017). To produce a species-mean neurocranium and otic neurocranium shape for figures, the mean position of landmark coordinates of all species in our data set was calculated with the 'mshape' function of 'geomorph' (Adams *et al.*, 2016), and the 'tps3d' function in the 'Morpho' library (Schlager, 2015) was used to deform a neurocranium and otic neurocranium surface file to the mean shape. We used the 'tps3d' function in 'Morpho' (Schlager, 2015) to produce superimposed representations of the shape of neurocrania and otic neurocrania on the extremes of PC axes.

Phylogenetic signal

We estimated phylogenetic signal in shape data with the multivariate *K*-statistic (Adams, 2014) using the Procrustes coordinate data for the full neurocranium and for auditory neurocranium datasets. These tests were applied using the 'physignal' function of 'geomorph' (Adams *et al.*, 2016). In addition, we examined phylogenetic signal present on the individual PC axes that contributed to at least 75% of the cumulative variation with a univariate lambda test (Ives *et al.*, 2007) with the 'phylosig' function in the 'phytools' library (Revell, 2012).

Modularity of the otic neurocranium

We tested for modularity of the otic region of the neurocranium relative to the other neurocranium landmarks. We used the covariance ratio (CR) test of Adams (2016). This test measures the degree of independence between structures (modularity) by examining the covariance within and among modules. We conducted this test with the 'modularity.test' function in 'geomorph' (Adams *et al.*, 2016) and used 999 iterations to assess significance by randomization of landmark subsets between modules. In addition, to account for potential effects of phylogenetic history on the degree of observed modularity among species, we performed the same test under a Brownian motion model of evolution using the 'phylo.modularity' function in 'geomorph' (Adams *et al.*, 2016).

Shape allometry

We performed several tests to determine if the shape relationships among species in our study were influenced by size. Using the 'stats' package in R, we performed Pearson correlation tests between the log10-transformed means of centroid size for the neurocranium and otic neurocranium and the PC axes that explained at least 75% of the shape variation. In addition, for both the neurocranium and the otic neurocranium, we performed a Procrustes regression to test for patterns of shape covariation among species using the 'procD.allometry' function of 'geomorph' (Adams *et al.*, 2016). These models used the natural log transformation of mean centroid size for each species and initially included an interaction with ecological

Downloaded from https://academic.oup.com/biolinnean/advance-article-abstract/doi/10.1093/biolinnean/bly092/5057832
by Natural History Museum user
on 24 July 2018

group, which was dropped from the model if not significant. Lastly, we considered phylogeny in tests of size covariation with shape. We used the 'procD.pgls' function of 'geomorph' (Adams *et al.*, 2016) to perform phylogenetic generalized least squares (PGLS) Procrustes regressions for the neurocranium and otic neurocranium. We tested models with and without an ecological group interaction term and used the natural log of mean centroid size for each species.

Shape convergence

To test for putative cases of convergent evolution of neurocranium shape, we used the approach of Stayton (2017) to test for pattern-based similarity by quantifying the amount of phenotypic distance between lineages closed by evolution. After examination of phylomorphospace plots from PCA and between-groups PCA (bgPCA), we identified two examples of putative convergence. We used the 'convratsig' function of the 'convevol' package (Stayton 2017) in R to calculate the proportion of the maximum phenotypic distance between putatively convergent taxa closed by evolution (C_1), the magnitude of phenotypic distance closed by evolution (C_2), the proportion of the magnitude of convergence relative to the phenotypic distance of the lineages being compared (C_3), and the proportion of the magnitude of convergence relative to the phenotypic distance of all lineages descended from the most recent common ancestor of the putatively convergent taxa (C_4) (Stayton, 2017). For both cases of putatively convergent taxa, we tested convergence among total neurocranium shape and total otic neurocranium shape by using PCA scores (all axes that together described at least 75% of variation) to calculate phenotypic distance with 'convratsig'. In addition, we performed two additional tests of convergence of the shape features associated with the greatest separation among ecological groups for the entire neurocranium and otic neurocranium using the scores from the bgPCAs. To calculate statistical significance of measures of convergence ($C_{1\text{-}4}$), we performed 1000 simulations.

Shape–ecology relationships

We tested for relationships between overall shape of the neurocranium and the auditory neurocranium and ecology using phylogenetic MANOVA tests (Garland *et al.*, 1993) on the PC axes that collectively explained ≥ 75% of variation. These tests were conducted with the 'aov.phylo' function of the 'geiger' library (Harmon *et al.*, 2015) in R (R Core Team, 2017). For these tests, we ran 1000 simulations and used Wilk's lambda as our multivariate test. In cases where differences were detected among groups ($P < 0.05$) from the 1000 simulations, we used the 'phylANOVA' function to perform phylogenetic ANOVA followed by Holm's post-hoc test using the 'phytools' package.

We used bgPCA to determine which subset of shape features best discriminate the a priori-defined ecological groups. This method produces orthogonal axes and avoids the problems of small within-group sample sizes and high-dimensional geometric morphometric data for analyses such as Canonical Variates Analysis (Mitteroecker & Bookstein, 2011). The bgPCA uses the co-variance matrix of the means of a priori-defined groups, and then projects the individual data on to the eigenspace defined by the between-group covariance matrix (Mitteroecker & Bookstein, 2011; Schlager, 2015). Two bgPCAs were performed, one on the entire neurocranium landmark dataset, and one on the subset of landmarks associated with the auditory region of the skull. To perform these analyses, we used the 'groupPCA' function of the 'Morpho' library (Schlager, 2015). Species scores from the two axes of the bgPCA were plotted as a phylomorphospace using the 'phylomorphospace' function in the 'phytools' library (Revell, 2017) in R (R Core Team, 2017). We used the 'tps3d' function in 'Morpho' (Schlager, 2015) to produce superimposed representations of the shape of neurocrania and otic neurocrania on the extremes of bgPC axes. Differences among the Euclidean distances of the bgPCA scores from the three groups were tested by permutation (10 000 rounds) in 'Morpho'. We also tested for differences among bgPCA scores of the three groups while accounting for phylogeny with a phylogenetic MANOVA and for post-hoc comparisons used phylogenetic ANOVA and Holm's tests as described above.

Morphological disparity among ecological groups

Morphological disparity was measured for the entire neurocranium landmark dataset and the subset of landmarks from the auditory region. To perform these analyses, we used the 'morphol.disparity' function of the 'geomorph' library (Adams *et al.*, 2016). The Procrustes variance estimate is a measure of the sum of the diagonal elements of the group covariance matrix divided by sample size (Adams *et al.*, 2016).

RESULTS

Overall neurocranium shape

The first three principal components (PCs) explained 52, 14 and 10% of the variation in neurocranium shape and the first five PCs explained 90% of the cumulative variation (Fig. 3, Table 2).

Downloaded from https://academic.oup.com/biolinnean/advance-article-abstract/doi/10.1093/biolinnean/bly092/5057832
by Natural History Museum user
on 24 July 2018

Phylogenetic signal was evident on the first three PCs (Fig. 3) as revealed by the univariate λ (Table 2). In addition, the multivariate *K*-statistic indicated significant phylogenetic signal for overall neurocranium shape (K_{mult} = 0.82, P = 0.001).

No evidence of allometry of neurocranium shape among species was observed. Correlations of centroid size of neurocranium landmarks and PC scores among species were weak (Table 2). Procrustes regression indicated no shape covariation with size among species ($F_{1,18}$ = 0.582, P = 0.702, R^2 = 0.031) and no interaction between size and ecological group was observed (P = 0.05). Similarly, after accounting for phylogeny with PGLS regression, no relationship between size and shape was observed ($F_{1,18}$ = 1.035, P = 0.230, R^2 = 0.068) and no interaction with size and ecology was observed (P > 0.05).

PC1 varied largely with respect to the relative height of the supraoccipital crest, length of the snout/mesethmoid region, size and anterior position of the orbit, length of the pterotic spine, and angle of the parasphenoid (Fig. 3). Both ecological groups and members of the three major serrasalmid clades were widely distributed along PC1 (Fig. 3A, B). Carnivores and frugivore/granivores displayed wide variation in shape features associated with PC1. For example, the relative elongate skull of the carnivore *Serrasalmus elongatus* Kner, 1858, which has a short supraoccipital crest, had the lowest score on PC1, while the carnivore *Catoprion mento* (Cuvier, 1819), which is relatively deep and has a tall supraoccipital crest, had the highest score among carnivores and the third highest score of all taxa on PC1 (Fig. 3A). PC2 varied largely with respect to the relative size of the orbit, anterior and lateral extent of the orbit, and relative size of the lagenar bulla (Fig. 3). High scores on PC2, associated with anteriorly positioned eyes and large lagenar bullae, separated carnivores from rheophilic herbivores, while frugivore/granivores were broadly distributed along PC2 (Fig. 3A, E). Major serrasalmid clades were largely distinguished along PC2, with low scores associated with *Myleus*-pacus, moderate scores associated with piranha clade members, and high scores associated with the pacu clade (Fig. 3B). High scores on PC3 were associated with a large pterotic spine and low scores were associated with a curved parasphenoid that descends ventrally (Fig. 3E). Carnivores were distinguished from rheophilic herbivores and most frugivore/granivores by high scores on PC3 (Fig. 3C). Major serrasalmid clades were distributed broadly across PC3 (Fig. 3D). For example, *Metynnis hypsauchen* (Müller & Troschel, 1844) and *M. lippincottianus* (Cope, 1870) had lower scores than the other members of the piranha clade, which were probably associated with their short pterotic spines.

PCA revealed (Fig. 3) overall shape similarity between *C. mento* of the piranha clade and *Myleus asterias* (Müller & Troschel, 1844), *Myloplus rubripinnis* (Müller & Troschel, 1844) and *Myloplus schomburgkii* (Jardine, 1844) of the *Myleus*-pacu clade. This observation was supported by measures of convergence higher than expected by chance (C_1 = 0.481, P < 0.001; C_2 = 0.079, P < 0.001; C_3 = 0.049, P < 0.001; C_4 = 0.059, P < 0.001). Both lineages are characterized by a deep skull, with high supraoccipital crest (Fig. S3). *Catoprion mento*, however, is characterized by a longer, straighter pterotic spine (Fig. S2). *Metynnis lippincottianus* and *M. hypsauchen* showed shape similarity with *Mylossoma aureum* (Spix & Agassiz, 1829) and *M. duriventre* (Cuvier, 1818) on PC1 and PC3 (Fig. 3). These two genera had a higher C_1 measure of convergence than expected by chance (C_1 = 0.291, P = 0.019), but other measures of convergence were not statistically significant (C_2 = 0.019, P = 0.262; C_3 = 0.012, P = 0.307; C_4 = 0.012, P = 0.307). Both genera are characterized by a slightly deeper skull and tall supraoccipital crest than average and a shorter pterotic spine (Fig. S3). *Metynnis*, however, differs from *Mylossoma* in having more dorsally orientated parasphenoid (Fig. S4). By contrast, *C. mento* diverged in shape from the elongate skull of *Pristobrycon striolatus* and *Serrasalmus elongatus*, and *Acnodon normani* was divergent in shape from other *Myleus*-pacus in having an elongate skull and large orbits (Fig. 3A, B).

Ecological group relationships to overall neurocranium shape

Phylogenetic MANOVA performed on PCs 1–3 indicated differences among ecological groups (Wilks λ = 0.12, $F_{2,17}$ = 9.40, $P_{non\text{-}phylo}$ < 0.001, P_{phyl} = 0.024). Phylogenetic ANOVA indicated a difference on PC3 between carnivore and frugivore/granivores ($F_{2,17}$ = 13.75, $P_{non\text{-}phylo}$ < 0.001, P_{phyl} = 0.036, Holmes post-hoc test P = 0.048), but not between rheophilic herbivores and carnivores (P = 0.214).

Between-group PCA of the overall neurocranium shape indicated that carnivores were best distinguished from frugivore/granivores along bgPC1 and were characterized by having a more anteriorly positioned orbit, a straight parasphenoid with an orientation mainly along the rostro-caudal axis, an elongate pterotic spine and lagenar bullae in a more dorsal position (Fig. 4). High scores on bgPC1 were also characterized by a neurocranium that was less deep and associated with a smaller supraoccipital crest. This morphology was present among some carnivore species (*Pristobrycon striolatus* [Steindachner, 1908], *S. elongatus*, *S. rhombeus*) (Fig. 4). Rheophilic herbivores were best distinguished from carnivores

Downloaded from https://academic.oup.com/biolinnean/advance-article-abstract/doi/10.1093/biolinnean/bly092/5057832
by Natural History Museum user
on 24 July 2018

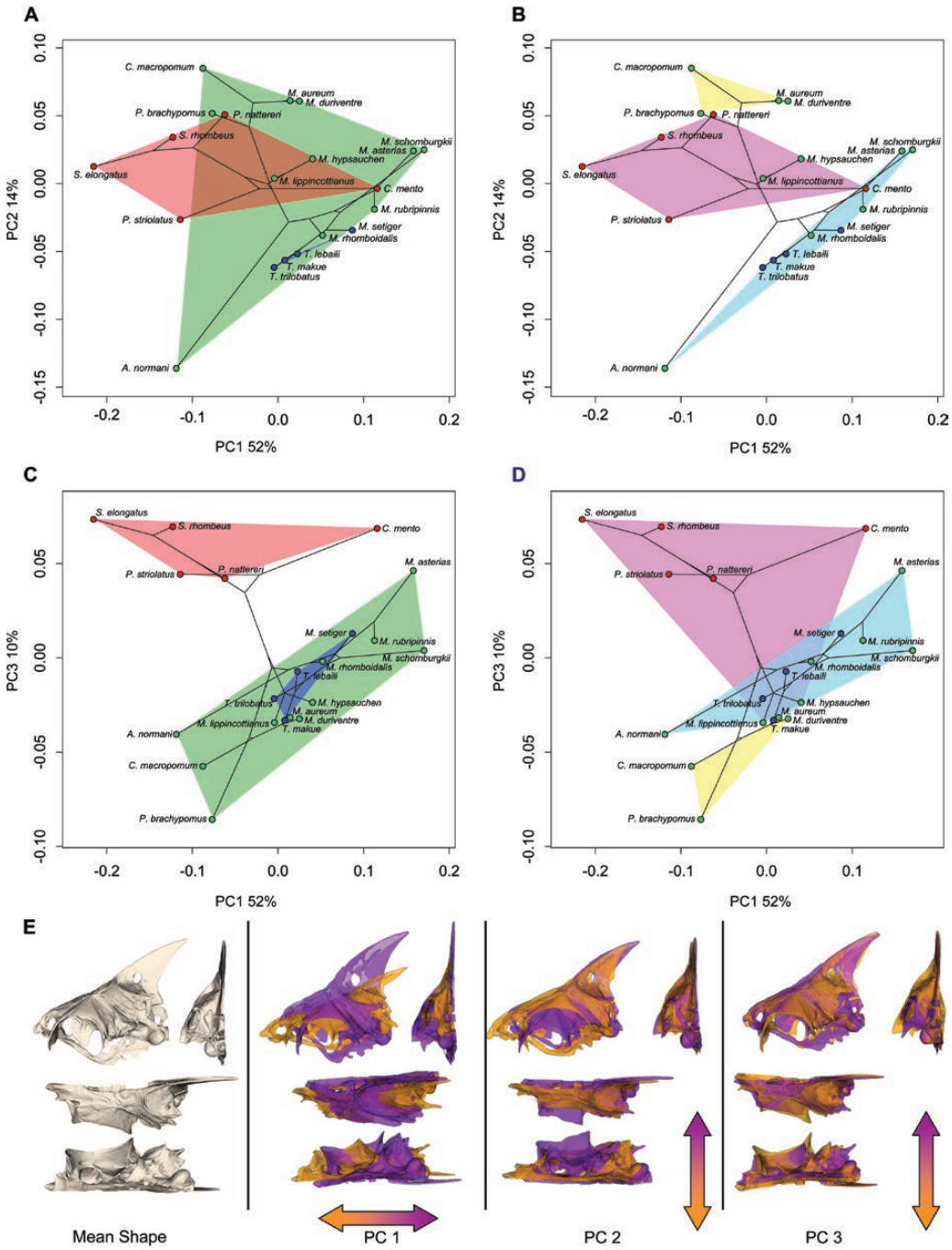

Figure 3. Overall shape variation of serrasalmid neurocrania revealed by principal components analysis (PCA). Phylomorphospace biplots of (A, B) principal components (PCs) 1 and 2 and (C, D) PCs 1 and 3. A, phylomorphospace with ecological groups outlined with minimum convex polygons (green = frugivore/granivores, blue = rheophilic herbivores, red = carnivores) shows broad overlap of frugivore/granivores and other groups on PCs 1 and 2, while rheophilic herbivores are distinguished from carnivores by lower scores on PC2. B, biplot of PCs 1 and 2 with three major serrasalmid clades outlined (yellow = pacu clade, light blue = *Myleus*-pacu clade, pink = piranha clade) shows overlap of all three clades on PC1, but more separation at the clade level on PC2. C, carnivores are separated from rheophilic herbivores and most frugivore/granivores along PC3. D, wide variation exists among the piranha clade along PC3, while most members of the pacus clade are distinguished from *Myleus*-pacus and piranha clade members by low scores on PC3. E, superimposed neurocrania surfaces indicate the shapes associated with the extremes of the PC axes: purple shapes = positive extremes, orange shapes = negative extremes. The mean shape of all species in the study is shown on the left in panel E. Top left, lateral view (anterior to the right); top right, caudal view (lateral to the left); middle, dorsal view (anterior to the right); bottom, ventral view (anterior to the right).

Downloaded from https://academic.oup.com/biolinnean/advance-article-abstract/doi/10.1093/biolinnean/bly092/5057832
by Natural History Museum user
on 24 July 2018

Table 2. Summary of the variation of principal component (PC) analyses on the geometric morphometric data, univariate lambda tests of phylogenetic signal conducted on individual PC axes, and correlations between mean centroid size and shape (PC score) on each axis

Structure	PC	Variation (%)	Cumulative %	Univariate phylogenetic signal		Pearson's product-moment correlation between centroid size of species and PC score			
				λ	*P*	*r*	*t*	d.f.	*P*
Neurocranium	PC1	52.1	52.1	**1.011**	**0.037**	0.23	0.98	18	0.340
	PC2	14.3	66.4	**1.108**	**< 0.001**	0.25	1.12	18	0.278
	PC3	10.1	76.5	**1.026**	**< 0.001**	–0.10	–0.44	18	0.669
	PC4	9.4	85.9						
	PC5	3.9	89.9						
Neurocranium Otic Region	PC1	45.9	45.9	**1.101**	**0.005**	0.31	1.38	18	0.186
	PC2	16.0	62.0	**1.015**	**< 0.001**	–0.19	–0.83	18	0.417
	PC3	9.2	71.2	**1.017**	**0.021**	0.25	1.07	18	0.296
	PC4	7.3	78.5	0.261	0.540	–0.38	–1.77	18	0.094
	PC5	6.1	84.6						

Bold type indicates statistical significance ($P < 0.05$).

along bgPC2, while frugivore/granivores displayed wide variation along this axis (Fig. 4). High scores on bgPC2 were characterized by a more anteriorly directed nasal region, larger and more posteriorly positioned orbits, a supraoccipital crest with less dorsal extension and extended more broadly posteriorally, and small lagenar bullae (Fig. 4). *Acnodon normani*, which has large orbits and a neurocranium that is less deep than most serrasalmids, had the highest scores on bgPC2, despite having large lagenar bullae. Permutation tests on the Euclidean distances of bgPCA scores indicated significant differences between carnivores and frugivore/granivores ($P = 0.018$) and between carnivores and rheophilic herbivores ($P = 0.038$), but not between rheophilic herbivores and frugivore/granivores ($P = 0.41$). However, differences among bgPCA scores of ecological groups were not evident after accounting for phylogeny (phyMANOVA Wilks $\lambda = 0.27$, $F_{2,17} = 7.35$, $P_{\text{non-phylo}} < 0.001$, $P_{\text{phyl}} = 0.089$).

As was observed for the overall neurocranium morphology identified by the standard PCA, *C. mento* showed convergence in neurocranium morphology identified by bgPCA to *M. asterias*, *M. rubripinnis* and *M. schomburgkii*. Measures of convergence were higher than expected by chance ($C_1 = 0.511$, $P = 0.003$; $C_2 = 0.063$, $P = 0.001$; $C_3 = 0.060$, $P < 0.001$; $C_4 = 0.070$, $P < 0.001$). In addition, *Metynnis* and *Mylossoma* had a higher C_1 measure of convergence than expected by chance ($C_1 = 0.464$, $P = 0.004$), but other measures of convergence were not statistically significant ($C_2 = 0.029$, $P = 0.091$; $C_3 = 0.028$, $P = 0.071$; $C_4 = 0.028$, $P = 0.071$).

Overall neurocranium shape disparity

Carnivores had the greatest overall neurocranium shape disparity (Procrustes variance = 27.49×10^{-3}), followed by frugivore/granivores (19.20×10^{-3}) and rheophilic herbivores (8.33×10^{-3}). The overall observed variation (sum of group covariance matrix diagonal elements) was highest for carnivores (0.1100), followed by frugivore/granivores (0.0768) and rheophilic herbivores (0.0333). A permutation test did not reveal significant differences in disparity among ecological groups ($P > 0.05$ for all comparisons). Among the three clades, the piranha clade had the greatest shape disparity (22.73×10^{-3}, observed variation 0.0909), followed by the *Myleus*-pacu clade (17.99×10^{-3}, observed variation 0.0719) and the pacu clade (15.24×10^{-3}, observed variation 0.0609). A permutation test did not reveal statistically significant differences in disparity among clades ($P > 0.05$ for all comparisons).

Shape of the otic neurocranium

The otic and non-otic regions of the neurocranium showed a significant degree of modularity. CR was 0.955 ($P = 0.001$) for the non-phylogenetic model and 0.977 ($P = 0.001$) for the phylogenetic model.

The first three PCs from a PCA performed on a subset of neurocranium landmarks of the otic region explained 46, 16 and 9% of the variation in neurocranium shape and the first five PCs explained 85% of the cumulative variation (Fig. 5, Table 2).

Phylogenetic signal of otic neurocranium shape was evident on PCs 1–3 (Fig. 5) as revealed by the univariate λ (Table 2). In addition, the multivariate *K*-statistic

Downloaded from https://academic.oup.com/biolinnean/advance-article-abstract/doi/10.1093/biolinnean/bly092/5057832
by Natural History Museum user
on 24 July 2018

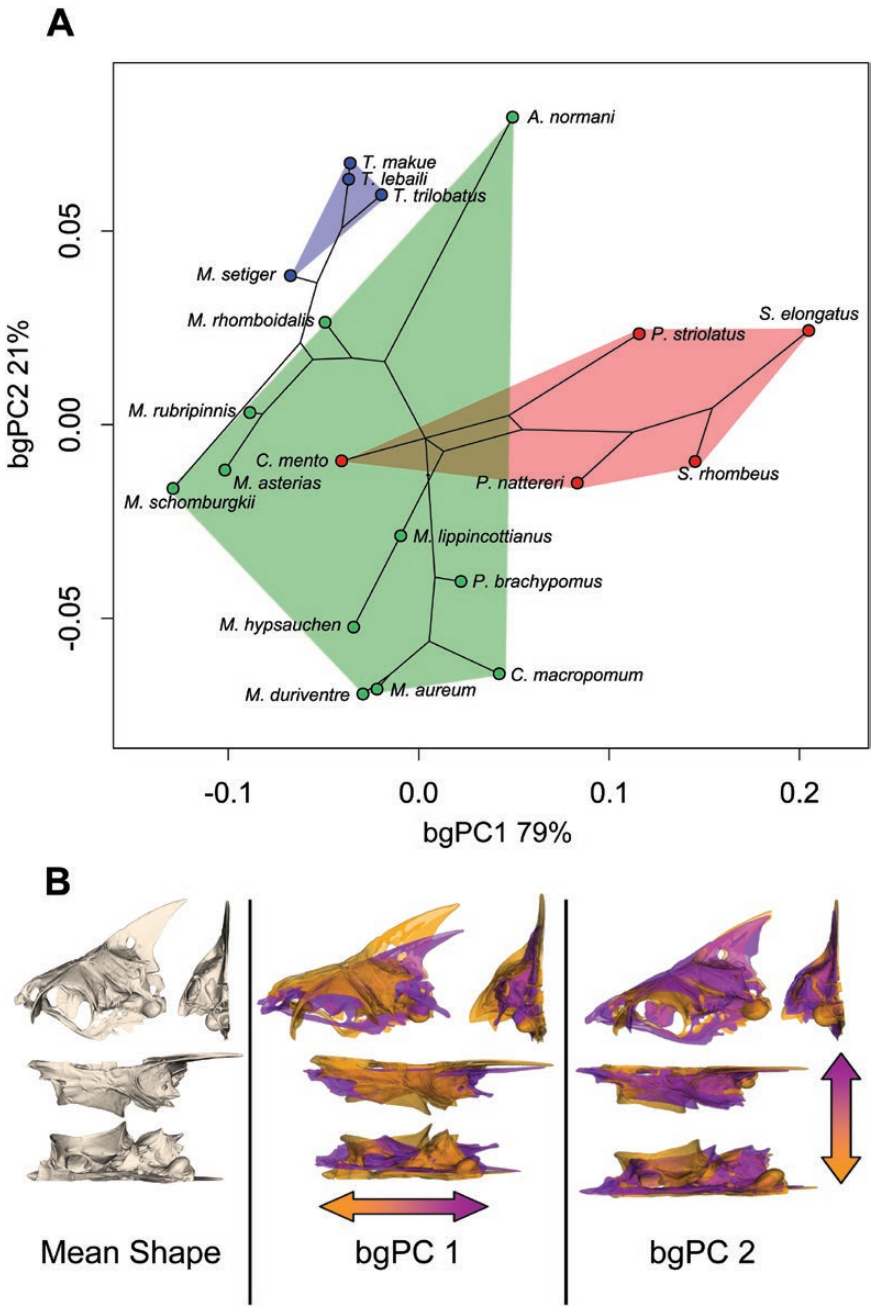

Figure 4. A, between-group principal components analysis (bgPCA) to determine the features of the overall neurocranium landmark dataset that best distinguish ecological groups. Carnivores (red polygons) are distinguished from rheophilic herbivores (blue) by low scores on bgPC2, while frugivore/granivores (green) overlapped in morphospace with carnivores and rheophilic herbivores on bgPCs 1 and 2. B, superimposed neurocrania surfaces indicate the shapes associated with the extremes of the bgPC axes: purple shapes = positive extremes, orange shapes = negative extremes. The mean shape of all species in the study is shown on the left in panel B. Left, lateral view (anterior to the right); middle, caudal view (lateral to the left); top right, dorsal view (anterior to the right); bottom right, ventral view (anterior to the right).

indicated significant phylogenetic signal (K_{mult} = 0.75, P = 0.001).

No evidence of allometry of otic neurocranium shape among species was observed. Correlations of centroid size of otic neurocranium landmarks and PC scores among species were weak (Table 2). Procrustes regression indicated no shape covariation with size among species ($F_{1,18}$ = 1.00, P = 0.372, R^2 = 0.053) and

Downloaded from https://academic.oup.com/biolinnean/advance-article-abstract/doi/10.1093/biolinnean/bly092/5057832
by Natural History Museum user
on 24 July 2018

no interaction between size and ecological group was observed (P = 0.05). After accounting for phylogeny with PGLS regression, no relationship between size and shape among species was observed ($F_{1,18}$ = 1.22, P = 0.280, R^2 = 0.064). However, an interaction between ecological group and size was observed ($F_{1,2,2,14}$ = 2.25, P = 0.007, R^2 = 0.205). This interaction appears to be influenced by shape divergence between carnivores and rheophilic herbivores that have otic neurocrania of similar size and broad shape and size variation of the otic neurocrania of frugivore/granivores (Fig. S4).

High scores on PC1 were associated with a relatively small lagenar bulla, a large vertebral articulation of the basioccipital, and anteriorly positioned prootic and nVII foramina (Fig. 5A, E). Frugivore/granivores were widely distributed along PC1, while carnivores and rheophilic herbivores were less distributed along this axis of shape space and did not overlap with each other (Fig. 5A). Of the major serrasalmid clades, the *Myleus*-pacus clade was broadly distributed along PC1, while the piranha and pacu clades occupied more narrow, and largely non-overlapping regions along PC1 (Fig. 5B). Low scores on PC2 were associated with more posteriorly positioned lagenar bullae and anteriorly positioned prootic and nVII foramina, and a more anteriorly positioned opening of the cavum sinus impar (Fig. 5E). All ecological groups overlapped on PC2, with rheophilic herbivores tending to have higher PC2 scores than carnivores (Fig. 5A). Major serrasalmid clades overlapped along the PC2 shape axis, with the highest scores exhibited within the *Myleus*-pacus clade (Fig. 5B). Low scores on PC3 were associated with larger lagenar bullae, a smaller and rounder vertebral articulation surface of the basioccipital, and posteriorly positioned prootic and nVII foramina (Fig. 5E). Rheophilic herbivores had higher scores than carnivores along PC3, while frugivore/granivores were broadly distributed along this axis (Fig. 5C). All three major serrasalmid clades were broadly distributed and largely overlapping along PC3 (Fig. 5D).

In contrast to the pattern observed for the entire neurocranium, *C. mento* did not display shape convergence of the otic neurocranium with *M. asterias*, *M. rubripinnis* and *M. schomburgkii* (C_1 = 0.069, P = 0.440; C_2 = 0.006, P = 0.488; C_3 = 0.004, P = 0.539; C_4 = 0.006, P = 0.519). *Catoprion mento* is characterized by an expanded lagenar bulla and a longer prootic with a greater distance between the lagenar bulla and the prootic and nVII foramina relative to these *Myleus*-pacu species (Fig. S2). Convergence of otic neurocranium morphology between *Metynnis* and *Mylossoma* was observed, as was seen previously for the overall neurocranium (C_1 = 0.301, P = 0.005; C_2 = 0.037, P = 0.007; C_3 = 0.026, P = 0.010; C_4 = 0.026, P = 0.010). Both *Metynnis* and *Mylossoma* are characterized by a larger lagenar bulla and more anteriorly positioned prootic foramen and nVII foramen (Fig. S3).

Ecological group relationships to otic neurocranium shape

A MANOVA performed on the first four PCs indicated differences among ecological groups (Wilks λ = 0.21, $F_{2,17}$ = 4.07, $P_{non\text{-}phylo}$ = 0.003), but these differences were not significant after accounting for phyogenetic history (phyMANOVA, P_{phyl} = 0.361). Differences were also not observed on individual PC axes (1–4), however, when tested with ANOVA (P > 0.05).

Between-group PCA of the otic region of the neurocranium indicated that carnivores were best distinguished from rheophilic herbivores along bgPC1 and were characterized by larger lagenar bullae that extended more ventrally, a smaller and rounder vertebral articulation of the basioccipital, a taller opening of the cavum sinus impar, and a prootic foramen that is positioned more caudally (Fig. 6). Frugivore/granivores were best distinguished from carnivores and rheophilic herbivores by lower scores along bgPC2 and were characterized by having the largest lagenar bullae, a shallower opening of the cavum sinus impar and a prootic foramen that was wider laterally (Fig. 6). Permutation tests on the Euclidean distances of bgPCA scores indicated significant differences between carnivores and rheophilic herbivores (P = 0.022), but not between carnivores and frugivore/granivores (P = 0.272) or between rheophilic herbivores and frugivore/granivores (P = 0.056). Differences in the auditory region of the neurocranium were observed after accounting for phylogeny (Wilks λ = 0.09, $F_{2,17}$ = 18.57, $P_{non\text{-}phylo}$ < 0.001, P_{phyl} = 0.002). Differences along bgPC1 were not observed after accounting for phylogeny (phyANOVA $F_{2,17}$ = 7.84, $P_{non\text{-}phylo}$ = 0.004, P_{phyl} = 0.139). Shape differences were, however, evident along bgPC2 after accounting for phylogeny (phyANOVA $F_{2,17}$ = 29.56, $P_{non\text{-}phylo}$ < 0.001, P_{phyl} = 0.004): frugivore/granivores differed from rheophilic herbivores and carnivores (Holme's post-hoc test P = 0.018 for both).

Catoprion mento did not display shape convergence of otic neurocranium morphology identified by bgPCA with *M. asterias*, *M. rubripinnis* and *M. schomburgkii* (C_1 = 0.204, P = 0.248; C_2 = 0.011, P = 0.376; C_3 = 0.013, P = 0.408; C_4 = 0.017, P = 0.388). *Metynnis* and *Mylossoma*, however, were convergent in otic neurocranium morphology identified from bgPCA (C_1 = 0.375, P = 0.023; C_2 = 0.030, P = 0.032; C_3 = 0.036, P = 0.030; C_4 = 0.036, P = 0.030).

Downloaded from https://academic.oup.com/biolinnean/advance-article-abstract/doi/10.1093/biolinnean/bly092/5057832
by Natural History Museum user
on 24 July 2018

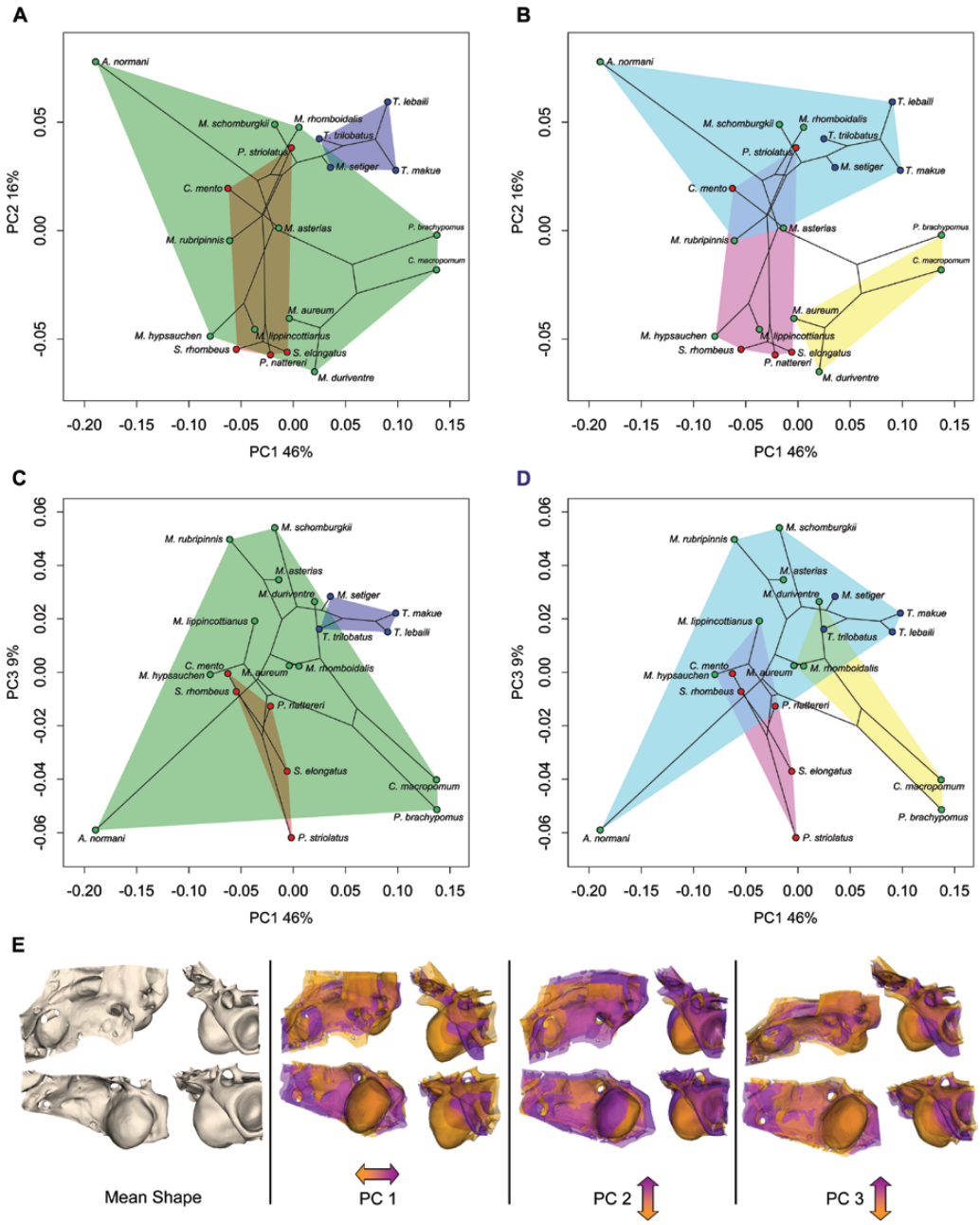

Figure 5. Shape variation of the otic region of serrasalmid neurocrania revealed by PCA. Phylomorphospace biplots of (A, B) principal components (PCs) 1 and 2 and (C, D) PCs 1 and 3. A, phylomorphospace with ecological groups outlined with minimum convex polygons (green = frugivore/granivores, blue = rheophilic herbivores, red = carnivores) shows broad overlap of frugivore/granivores with rheophilic herbivores and carnivores on PCs 1 and 2, while carnivores are distinguished from rheophilic herbivores on PC1, but not PC2. B, biplot of PCs 1 and 2 with three major serrasalmid clades outlined (yellow = pacu clade, light blue = *Myleus*-pacu clade, pink = piranha clade) shows that members of the pacu clade are largely distinguished from piranha clade members along PC1, while pacu clade members are largely distinguished from *Myleus*-pacu clade members along PC2. C, frugivore/granivores are widely distributed along PC3 and overlap both carnivores and rheophilic herbivores. Carnivores are distinguished from rheophilic herbivores by lower scores on PC3. D, all three major serrasalmid clades show broad overlap along PC3. E, superimposed otic neurocranium region surfaces indicate the shapes associated with the extremes of the PC axes: purple shapes = positive extremes, orange shapes = negative extremes. The mean shape of all species in the study is shown on the left in panel E. The rendered surface includes portions of the prootic, exoccipital and basioccipital, while the parietal, frontal and supraoccipital have been removed. Top left, dorsal view of the

Downloaded from https://academic.oup.com/biolinnean/advance-article-abstract/doi/10.1093/biolinnean/bly092/5057832
by Natural History Museum user
on 24 July 2018

Otic neurocranium shape disparity

Frugivore/granivores had the greatest shape disparity (Procrustes variance = 14.28×10^{-3}, observed variation 0.0571), followed by rheophilic herbivores (9.95×10^{-3}, observed variation 0.0398) and carnivores (9.83×10^{-3}, observed variation 0.0393). A permutation test did not reveal statistically significant differences in disparity among clades ($P > 0.05$ for all comparisons). Among the three clades, the pacu clade had the greatest shape disparity (15.20×10^{-3}, observed variation 0.0608) followed by the *Myleus*-pacus (13.03×10^{-3}, observed variation 0.0521) and the piranha clade (9.72×10^{-3}, observed variation 0.0389). A permutation test did not reveal statistically significant differences in disparity among clades ($P > 0.05$ for all comparisons).

DISCUSSION

This study demonstrated that serrasalmid neurocranium morphology is influenced by both phylogeny and ecology and that some shape aspects are associated with ecology after accounting for evolutionary history. In addition, the otic and non-otic neurocranium are modular and the otic neurocranium module is influenced by phylogeny and ecology after accounting for phylogeny. Neurocranium shape variation is associated principally with the depth of the skull, the size and position of the orbit, the length of the pterotic spine, and the relative size of the lagenar bulla. This observed variation in neurocranium shape was not explained by variation in size and no evidence of shape allometry was observed. Dorsal elongation of the skull, resulting from expansion of the supraoccipital crest and ventral expansion of the parasphenoid, has evolved repeatedly within the Serrasalmidae, occurring in each of the three major clades and the frugivore/granivore and carnivore ecological groups. Several areas of observed variation are probably correlated with sensory roles and may be related to ecology: elongation of the nasal region, position and size of the orbit, and relative size of the lagenar bulla. Evidence of modularity between otic and non-otic neurocranium regions indicates that the function of the ear may have influenced the shape evolution of this region independently relative to other regions of the neurocranium. The restricted analysis of the otic region of the neurocranium indicated strong differences among ecological groups associated with the size of the lagenar bulla, the relative position of the bulla with regard to the basioccipital – vertebra 1 articulation, and the rostro-caudal position of the two foramina of the prootic. Lastly, there is a strong phylogenetic trend associated with some aspects of skull shape: laterally expanded orbits in the piranha and pacu clade, an elongate pterotic spine as a derived feature within the piranha clade, and anteriorly positioned lagenar bullae in *Myleus*-pacu clade members.

In this study, a major axis of shape variation related to depth and elongation of the skull was detected. This main axis of variation has been observed in other studies of head shape in fishes, for example in populations of threespine stickleback *Gasterosteus aculeatus* (Pistore *et al.*, 2016). Relatively deep skulls were associated with a taller supraoccipital crest. Elaboration of the supraoccipital crest appears to be related to body depth in serrasalmids (Alexander, 1964). The increased height of vertebrae, neural spines and associated epaxial musculature requires a firm, large origin, as provided by the supraoccipital crest (Alexander, 1964). In this study, convergent deep neurocranium morphologies were observed between the lepidophagous carnivore *Catoprion mento* and several frugivore/granivores in the *Myleus*-pacu clade. However, these species differed in the length and shape of the pterotic spine and morphology of the otic neurocranium. Convergence in deep-bodied neurocrania was also observed in *Metynnis* and *Mylossoma*. In this study, deep skulls were often associated with a parasphenoid with a greater dorso-ventral extent. Serrasalmids show variation in body depth within each of the three major clades. Relatively elongate-bodied species occurred in the piranha clade (*Serrasalmus elongatus*, *Pristobrycon striolatus* and *S. rhombeus*) and in the *Myleus*-pacus clade (*Acnodon normani*). The degree of body depth vs. elongation is a major source of repeated evolutionary variation among teleost fishes (Ward & Brainerd, 2007; Friedman, 2010; Sallan & Friedman, 2012; Claverie & Wainwright, 2014). Among other distantly related teleost lineages that vary in relative body length vs. depth, e.g. Anabantoidei, elongation of the head and skull is a main source of overall elongation (Collar *et al.*, 2016). This study found multiple examples of divergence between sister taxa along the axis of neurocranium depth and elongation: *C. mento* vs. *P. striolatus*, *Acnodon normani* vs. derived *Myleus*-pacus, and *Colossoma macropomum*.

Elongation of the neurocranium of serrasalmids in this study involved either extension of the nasal/ethmoid region or elongation of the otic region of the skull, the latter of which resulted in a relatively more anterior position of the eyes on the head. Anteriorly positioned orbits were characteristic of piranhas in this

bone overlying the sinus endolymphaticus (anterior is to the right); top right, caudal oblique dorsal view that shows the left portion of the cavum sinus impar (lateral to the left); bottom left, ventro-lateral view of the lagenar bulla and prootic with prootic and nVII foramina visible (anterior is to the right); bottom right, caudal view (lateral to the left).

Downloaded from https://academic.oup.com/biolinnean/advance-article-abstract/doi/10.1093/biolinnean/bly092/5057832
by Natural History Museum user
on 24 July 2018

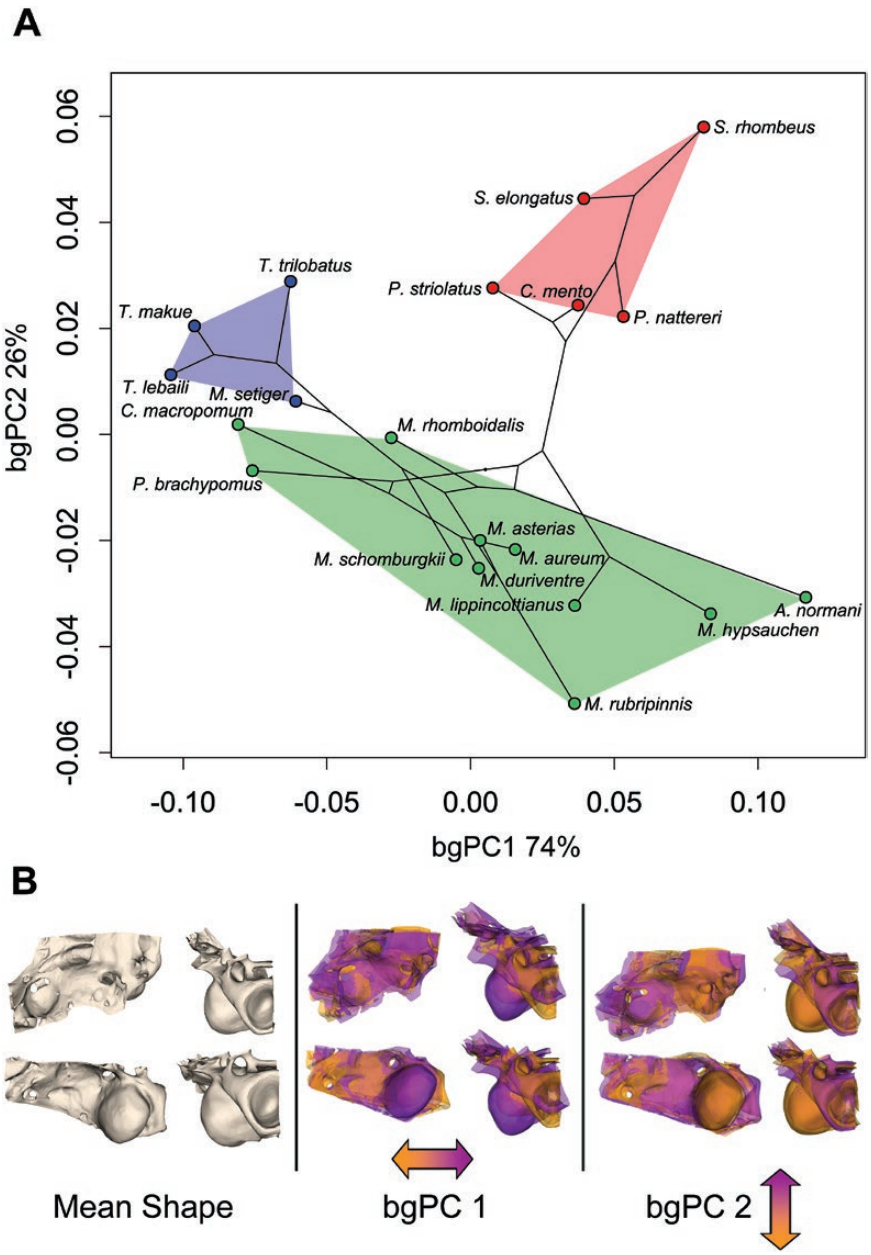

Figure 6. Between-group principal components analysis (bgPCA) to determine the features of the otic region of the neurocranium landmark dataset that best distinguish ecological groups. Carnivores (red polygons) are distinguished from rheophilic herbivores (blue) by low scores on bgPC2, while frugivore/granivores (green) overlapped in morphospace with carnivores and rheophilic herbivores on bgPCs 1 and 2. Superimposed neurocrania surfaces indicate the shapes associated with the extremes of the PC axes: purple shapes = positive extremes, orange shapes = negative extremes. Left, lateral view (anterior to the right); middle, caudal view (lateral to the left); top right, dorsal view (anterior to the right); bottom right, ventral view (anterior to the right). Superimposed otic neurocranium region surfaces indicate the shapes associated with the extremes of the PC axes: purple shapes = positive extremes, orange shapes = negative extremes. The mean shape of all species in the study is shown on the left in panel E. The rendered surface includes portions of the prootic, exoccipital and basioccipital, while the parietal, frontal and supraoccipital have been removed. Top left, dorsal view of the bone overlying the sinus endolymphaticus (anterior is to the right); middle, caudal oblique dorsal view that shows the left portion of the cavum sinus impar (lateral to the left); right, caudal view (lateral to the left); bottom left, ventro-lateral view of the lagenar bulla and prootic with prootic and nVII foramina visible (anterior is to the right).

Downloaded from https://academic.oup.com/biolinnean/advance-article-abstract/doi/10.1093/biolinnean/bly092/5057832
by Natural History Museum user
on 24 July 2018

study and may be predicted to be associated with the role of vision in the predatory habits of these species. Orbit position also affects the location of the suspensorium and hyomandibula articulation behind the orbit, and the location of the pterotic. These two features have ramifications for feeding because they affect the position of the lower jaw articulation and the length and angle of adductor mandibulae muscle fibres.

Several serrasalmids in this study were characterized by relatively large orbits. Eye size is correlated with visual acuity and habitat type (Caves *et al.*, 2017). *Acnodon normani* has a large orbit that is positioned at a large relative distance to the anterior end of the neurocranium. In addition, the cranium is relatively narrow in lateral aspect in this species. Piranha orbits also tended to be large, but, as mentioned above, were located further anteriorly.

One source of variation among serrasalmid skulls was the relative length of the pterotic spine. As noted by Alexander (1964), the pterotic spine reaches the level of the supracleithrum in piranhas. A long pterotic spine is a feature that was observed in all carnivores of the piranha clade and members of the pacu clade, especially *Colossoma macropomum* (Cuvier, 1816) and *Piaractus brachypomus* (Cuvier, 1818). A relatively short pterotic spine was present among most of the other frugivore/granivores in this study, including the frugivore/granivore members of the piranha clade (*Metynnis* spp.), as well as the rheophilic herbivores. The pterotic spine is the origin for some muscle fibres involved in closing the jaws. Some fibres of the pars malaris (originally A2) subdivision of the adductor mandibulae originate on the pterotic and pterotic spine of *Serrasalmus* (Alexander, 1964; Mirande, 2009; Datovo & Castro, 2012; Datovo & Vari, 2014). In *Serrasalmus* the pterotic spine provides part of the origin of the A2 subdivision of the adductor mandibulae (Alexander, 1964). Some A2 lateral fibres also originate on the pterotic spine (Datovo & Castro, 2012). Thus, future studies should examine if variation in the elaboration of this bone is associated with feeding and biting.

The orientation of the parasphenoid varies among serrasalmid species, from a near-horizontal orientation along the rostro-caudal axis, exhibited in species such as *Serrasalmus elongatus*, to an orientation that extends ventrally from rostral to caudal in *Metynnis* spp. and *Myleus* spp. Parasphenoid orientation also varied between taxa with neurocrania that were convergent in other aspects (*Metynnis* and *Mylossoma*). Variation in this orientation is apparent in the first two principal components of overall neurocranium shape (Fig. 3) and in the first axis of the analysis of overall shape between ecological groups (Fig. 4). Orientation of this bone may have implications in biting and prey processing. In *Serrasalmus* spp., some fibres of the A2 subdivision of the adductor mandibulae originate on the parasphenoid and pterosphenoid, and some fibres of the A3 adductor mandibulae originate on the parasphenoid, along with the pterosphenoid and metapterygoid (Datovo & Castro, 2012). In addition, in serrasalmids the parasphenoid is the origin of the adductor arcus palatini, which inserts on the dorsomedial face of the hyomandibula (Datovo & Castro, 2012). This muscle may be involved in compression of the buccal cavity during feeding and swallowing, as was observed in distantly related serrasalmids (Lauder, 1981). Future studies should examine if orientation of the parasphenoid in serrasalmids accompanies variation in muscle fibre length and orientation in the adductor mandibulae and adductor arcus palatini that may influence bite force and prey transport, respectively. In addition, orientation and length may have ramifications for neurocranium strength during feeding.

Otic neurocranium

In this study, the otic neurocranium varied according to both ecology and phylogeny. The observed modularity between otic and non-otic neurocranium regions is consistent with the hypothesis that hearing and vestibular sensory evolution has influenced the morphological evolution of the neurocranium. Patterns of convergence of the overall neurocranium and otic neurocranium are in agreement with the observed modularity. For example, convergence between *C. mento* and several *Myleus*-pacu clade members was apparent for the overall neurocranium in general, but not for the otic neurocranium. Serrasalmids, like most otophysans, are characterized by acute hearing and sound pressure sensitivity that exists because of the presence of a Weberian apparatus (Stabentheiner, 1988; Ladich, 1999; Mélotte *et al.*, 2018). In addition, serrasalmids have well-developed lagenar otoliths (asterisci), which in otophysan fishes are relatively large and associated with particle motion detection (Fay, 1984; Popper & Fay, 2011). Variation in the size of the lagenar bulla among ecological groups indicates that the importance of sound particle motion detection may vary with ecology. Small lagenar bullae in this study were associated with rheophilic herbivorous ecologies. These differences parallel differences in relative asteriscus size and shape differences observed in rheophilic herbivore serrasalmids (K. S. Boyle & A. Herrel, unpubl. obs.; K. S. Boyle *et al.*, unpubl. obs.). Sound particle motion has a greater relative impact in the acoustic nearfield, which extends far in aquatic environments at lower frequencies (Bass & Clark, 2003). Splash sounds that incorporate low-frequency elements may be important

Downloaded from https://academic.oup.com/biolinnean/advance-article-abstract/doi/10.1093/biolinnean/bly092/5057832
by Natural History Museum user
on 24 July 2018

particle motion stimuli for both frugivores/granivores and carnivores. Splash sounds from falling seeds and fruits are thought to be attractive to some serrasalmids (Gottsberger, 1978; Piedade *et al.*, 2006; Correa *et al.*, 2007; Parolin *et al.*, 2010). Splashing, which can occur from wounded prey and from the swimming activities of piranhas feeding, is attractive to piranhas (Markl, 1972; Stabentheiner, 1988; Mol, 2006). The small lagenar bullae of rheophilic herbivores indicates that particle motion detection may be less important. The feeding ecology of these species is herbivory of submerged aquatic plants (Podostemaceae) (Jégu & Dos Santos, 2002; Jégu *et al.*, 2002b; Jégu & Keith, 2005; Ortí *et al.*, 2008; Andrade *et al.*, 2013; Dary *et al.*, 2017). Sounds are not expected to be associated with this food resource and it is not known if much sound is produced by rheophilic herbivores feeding on these plants. Furthermore, rheophilic habitats are predicted to be noisy environments (Lugli & Fine, 2003, 2007; Tonolla *et al.*, 2011) and perhaps high levels of particle motion background noise would select for a smaller lagena and lagenar bulla. Smaller otoliths are predicted to respond differently than larger otoliths to sound, with larger otoliths likely to have a greater response to low frequencies (Lychakov & Rebane, 2000; Popper *et al.*, 2005). An alternative hypothesis is that rheophilic environments favour particle motion sensitivity at higher frequencies, and thus a smaller asteriscus, which does not require a large lagenar bulla. In addition, relative size differences of the asteriscus and surrounding lagenar bulla of rheophilic herbivores compared to other serrasalmids may be related to differences in balance and postural requirements of life in high-energy environments such as rapids. The otolithic end organs of teleost fishes are hypothesized to be multifunctional by providing both vestibular and hearing senses (Popper & Platt, 1993). A negative relationship is predicted to exist between otolith size and balance requirements in fishes, and is supported, in part, by the small otolith sizes of large pelagic fishes that are capable of rapid angular accelerations (Popper *et al.*, 2005). Serrasalmids in high-energy rheophilic environments may need to manoeuvre more rapidly in currents in eddies. Consistent with this hypothesis, the lapillus of the utricle of rheophilic herbivore serrasalmids has a smaller relative size than in frugivore/granivore species (K. S. Boyle & A. Herrel, unpubl. obs). Importantly, hypotheses regarding the function of lagenar bulla reduction related to particle motion hearing and balance requirements of rheophilic herbivorous lifestyles are not mutually exclusive.

A prootic foramen that is open to the utriculus is a synapomorphy of characiform fishes (Fink & Fink, 1981). In addition, a foramen providing passage for a ramus of the facial nerve exists on the prootic, anterior to the prootic foramen, which also exposes the utriculus. It is not known if these structures contribute to hearing or the degree to which the utriculus is involved in hearing in serrasalmids. Variation in the size and position of these foramina along the rostrocaudal axis was observed in this study. For example, the prootic foramen tended to be wider among frugivore/granivores than in the other ecological groups. These foramina were in a relatively anterior position in *Colossoma macropomum* and *Piaractus brachypomus* and were in a relatively posterior position in *Acnodon normani*. Notably, these foramina occur in a more intermediate position in *Mylossoma aureum* and *M. duriventre* relative to the closely related *C. macropomum* and *P. brachyopomus*. Anterior swim bladder diverticulae are present in *Mylossoma* spp. (Nelson, 1961). Moreover, some of these diverticulae approach moderately close to the prootic foramen (K. S. Boyle & A. Herrel, unpubl. obs.). Swim bladder extensions in other fishes can provide increased sensitivity to sound pressure (Yan *et al.*, 2000; Parmentier *et al.*, 2011; Tricas & Boyle, 2015). However, this function seems less plausible for an otophysan fish that already has sensitivity to sound pressure via the Weberian apparatus. Hearing thresholds have not yet been tested for serrasalmids of the genus *Mylossoma* and are needed to better understand this question.

The fluid-filled sinus connection between the Weberian ossicle linkage and ear, the cavum sinus impar, showed some variation among serrasalmids in this study. Frugivore/granivores tended to have a cavum sinus impar that was in a lower, more shallow position above the occiput. A functional hypothesis for this observed difference is not clear, but shape and position variation of this feature may be expected to co-vary with shape and size differences of the scaphia, which are in close association with this structure.

Neurocranium shape disparity

Differences in neurocranium disparity among ecological groups were modest, with carnivores displaying the greatest amount of shape disparity in this study, while rheophilic herbivores had the least disparity in overall neurocranium morphology. Disparity among the major clades was also comparable. The oldest lineage, the pacu clade, showed the least disparity. Note, however, that branch lengths to the most recent common ancestor among the three major clades are similar (Fig. S1). Pacu clade members have deep skulls, with long pterotic spines, and large lagenar bullae. Greater shape disparity in the piranha clade could be explained, in part, by the variation in body depth among carnivorous species, and the variation in pterotic spine length between carnivores and the frugivore/granivore species of *Metynnis*. Intermediate disparity in the *Myleus*-pacu clade can be accounted for by variation in skull elongation (e.g. elongate *Acnodon normani*, deep *Myloplus schomburgkii*)

Downloaded from https://academic.oup.com/biolinnean/advance-article-abstract/doi/10.1093/biolinnean/bly092/5057832
by Natural History Museum user
on 24 July 2018

and lagenar bulla size between rheophilic herbivores and frugivore/granivores in this clade. Contrasting patterns of disparity for other cranial and anterior skeletal shape features have been observed in other characiform fishes (Sidlauskas, 2008). In clades of comparable diversity, the more trophically diverse clade shows higher disparity as a result of the morphospace occupied by the tips of the phylogeny (Sidlauskas, 2008). In this study, the clade with the least disparity (pacu clade) was also the only clade with only one ecological group among its members, although this pattern was not observed for otic neurocranium diversity.

Otic neurocranium disparity among ecological groups and clades was also comparable. Carnivores showed the least otic neurocranium disparity (comparable to rheophilic herbivores), while frugivore/granivores showed the greatest disparity. Carnivores had consistently large lagenar bullae and little variation in the position of the prootic and nVII foramina. Frugivore/granivores displayed more variation in the placement of the prootic and nVII foramina. This variation was evident within the pacu clade, which showed more variation in the position of these foramina. The *Myleus*-pacu clade showed moderate variation in otic neurocranium disparity, in part because of the variation in lagenar bulla size between rheophilic herbivores and frugivore/granivore members of this clade.

CONCLUSION

This study examined three-dimensional neurocranium shape in serrasalmids. Shape variation of the skull exhibits strong phylogenetic signal and also variation in regions that may be predicted to have consequences for sensory biology, hydrodynamic and body shape functions, and jaw suspension and feeding. The otic region of the neurocranium exhibited differences among ecological groups that parallels observations of otolith size and shape differences in recent studies in serrasalmids. Morphological disparity was not dramatically different among ecological groups or the three major clades of the family, however. Furthermore, the pattern of disparity among ecological groups and clades was not consistent between the overall neurocranium landmark data and the subset of the otic region. These results suggest that patterns of variation of the overall neurocranium may not be parallel to patterns of variation of individual modules, such as the otic neurocranium. This is evident among the carnivorous piranhas, which show broad variation in skull elongation, but a conserved pattern of large lagenar bullae in the otic neurocranium. Future research is needed to determine the consequences of the observed skull shape variation on the functional morphology of locomotion, feeding and sensory ecology in these fishes.

ACKNOWLEGEMENTS

We thank Zora Gabsi, Philippe Keith and Patrice Pruvost (MNHN, CNRS UMR 7208) for assistance and access to MNHN specimen loans. We are grateful to Miguel Garcia Sanz and Patricia Wils from the AST-RX platform at MNHN (CNRS UMS 2700) for μCT scanning and training in Avizo. We thank four anonymous reviewers for their suggestions that improved the manuscript. This study was funded by a Marie-Skłodowska Curie fellowship (EU project 625039 – EvoMorphASIS).

REFERENCES

Adams DC. 2014. A generalized K statistic for estimating phylogenetic signal from shape and other high-dimensional multivariate data. *Systematic Biology* **63:** 685–697.

Adams DC. 2016. Evaluating modularity in morphometric data: challenges with the RV coefficient and a new test measure. *Methods in Ecology and Evolution* **7:** 565–572.

Adams D, Collyer M, Sherratt E. 2016. *Package 'geomorph'. R package version 2.1.7-1*. Available at: https://cran.r-project.org/package=geomorph (accessed 14 July 2018).

Alexander RM. 1962. The structure of the Weberian apparatus in the Cyprini. *Proceedings of the Zoological Society of London* **139:** 451–473.

Alexander RM. 1964. Adaptation in the skulls and cranial muscles of South American characinoid fish. *Zoological Journal of the Linnean Society* **45:** 169–190.

Andrade MC, Giarrizo T, Jégu M. 2013. *Tometes camunani* (Characiformes: Serrasalmidae), a new species of phytophagous fish from the Guiana Shield, rio Trombetas basin, Brazil. *Neotropical Ichthyology* **11:** 297–306.

Andrade MC, Machado VN, Jégu M, Farias IP, Giarrizzo T. 2017. A new species of *Tometes* Valenciennes 1850 (Characiformes: Serrasalmidae) from Tocantins-Araguaia River Basin based on integrative analysis of molecular and morphological data. *PLoS ONE* **12:** e0170053.

Aquino PPU, Colli GR. 2017. Headwater captures and the phylogenetic structure of freshwater fish assemblages: a case study in central Brazil. *Journal of Biogeography* **44:** 207–216.

Arratia G. 2003. Catfish head skeleton—an overview. In: Arratia G, Kapoor BG, Chardon M, et al., eds. *Catfishes*. Enfield: Science Publishers, Inc., 3–46.

Bass AH, Clark CW. 2003. The physical acoustics of underwater sound communication. In: Simmons AM, Popper AN, Fay RR, eds. *Acoustic communication*. New York: Springer, 240–254.

Bird NC, Hernandez LP. 2007. Morphological variation in the Weberian apparatus of Cypriniformes. *Journal of Morphology* **268:** 739–757.

Bookstein FL. 1997. Landmark methods for forms without landmarks: morphometrics of group differences in outline shape. *Medical Image Analysis* **1997:** 3.

Botton-Divet L, Houssaye A, Herrel A, Fabre AC, Cornette R. 2015. Tools for quantitative form description; an evaluation of different software packages for semi-landmark analysis. *PeerJ* **3:** e1417.

Downloaded from https://academic.oup.com/biolinnean/advance-article-abstract/doi/10.1093/biolinnean/bly092/5057832
by Natural History Museum user
on 24 July 2018

Caves EM, Sutton TT, Johnsen S. 2017. Visual acuity in ray-finned fishes correlates with eye size and habitat. *The Journal of Experimental Biology* **220:** 1586–1596.

Chardon M, Vandewalle P. 1997. Evolutionary trends and possible origin of the Weberian apparatus. *Netherlands Journal of Zoology* **47:** 383–403.

Clabaut C, Bunje PM, Salzburger W, Meyer A. 2007. Geometric morphometric analyses provide evidence for the adaptive character of the Tanganyikan cichlid fish radiations. *Evolution* **61:** 560–578.

Claverie T, Wainwright PC. 2014. A morphospace for reef fishes: elongation is the dominant axis of body shape evolution. *PLoS ONE* **9:** e112732.

Collar DC, Quintero M, Buttler B, Ward AB, Mehta RS. 2016. Body shape transformation along a shared axis of anatomical evolution in labyrinth fishes (Anabantoidei). *Evolution* **70:** 555–567.

Correa SB, Winemiller KO, López-Fernández H, Galetti M. 2007. Evolutionary perspectives on seed consumption and dispersal by fishes. *Bioscience* **57:** 748–756.

Dary EP, Ferreira E, Zuanon J, Röpke CP. 2017. Diet and trophic structure of the fish assemblage in the mid-course of the Teles Pires River, Tapajós River basin, Brazil. *Neotropical Ichthyology* **15:** e160173.

Datovo A, Castro RM. 2012. Anatomy and evolution of the mandibular, hyopalatine, and opercular muscles in characiform fishes (Teleostei: Ostariophysi). *Zoology (Jena, Germany)* **115:** 84–116.

Datovo A, Vari RP. 2014. The adductor mandibulae muscle complex in lower teleostean fishes (Osteichthyes: Actinopterygii): comparative anatomy, synonymy, and phylogenetic implications. *Zoological Journal of the Linnean Society* **171:** 554–622.

Eschmeyer WN, Fong JD. 2017. Species by family/subfamily in the catalog of fishes. Available at http://researcharchive.calacademy.org/research/ichthyology/catalog/SpeciesByFamily.asp.

Fay RR. 1984. The goldfish ear codes the axis of acoustic particle motion in three dimensions. *Science (New York, N.Y.)* **225:** 951–954.

Fink SV, Fink WL. 1981. Interrelationships of ostariophysan fishes (Ostariophysi). *Zoological Journal of the Linnean Society* **72:** 297–353.

Fitzgerald DB, Sabaj Perez MH, Sousa LM, Gonçalves AP, Lujan NK, Zuanon J, Winemiller KO, Lundberg JG. 2018. Diversity and community structure of rapids-dwelling fishes of the Xingu River: implications for conservation amid large-scale hydroelectric development. *Biological Conservation* **222:** 104–112.

Friedman M. 2010. Explosive morphological diversification of spiny-finned teleost fishes in the aftermath of the end-Cretaceous extinction. *Proceedings of the Royal Society B: Biological Sciences* **277:** 1675–1683.

von Frisch K. 1938. The sense of hearing in fish. *Nature* **141:** 8–11.

Frost GA. 1925. LXI.— A comparative study of the otoliths of the Neopterygian fishes (continued). *Journal of Natural History Series 9* **15:** 553–561.

Garland T Jr, Dickerman AW, Janis CM, Jones JA. 1993. Phylogenetic analysis of covariance by computer simulation. *Systematic Biology* **42:** 265–292.

Goatley CHR, Bellwood DR. 2009. Morphological structure in a reef fish assemblage. *Coral Reefs* **28:** 449–457.

Gottsberger G. 1978. Seed dispersal by fish in the inundated regions of Humaitá, Amazonia. *Biotropica* **10:** 170–183.

Goulding M. 1980. *The fishes and the forest: explorations in Amazonian natural history*. Los Angeles: University of California Press.

Goulding M, Carvalho ML. 1982. Life history and management of the tambaqui (*Colossoma macropomum*, Characidae): an important Amazonian food fish. *Revista Brasileira de Zoologia* **30:** 107–133.

Gregory WK. 1933. Fish skulls: a study of the evolution of natural mechanisms. *Transactions of the American Philosophical Society* **23:** 75–481.

Gunz P, Mitteroecker P, Bookstein FL. 2005. Semilandmarks in three dimensions. In: Slice DE, ed. *Modern morphometrics in physical anthropology*. New York: Kluwer Academic/Plenum Publishers, 73–98.

Hanken J, Hall BK. 1993. Mechanisms of skull diversity and evolution. In: *The skull*. Chicago: University of Chicago Press, 1–36.

Hanken J, Thorogood P. 1993. Evolution and development of the vertebrate skull: the role of pattern formation. *Trends in Ecology and Evolution* **8:** 10–15.

Harmon L, Weir J, Brock C, Glor R, Challenger W, Hunt G, FitzJohn R, Pennell M, Slater G, Brown J, Uyeda J, Eastman J. 2015. *geiger: Analysis of Evolutionary Diversification. version 2.0.6.* Available at https://cran.r-project.org/package=geiger.

Helfman G, Collette BB, Facey DF, Bowen BW. 2009. *The diversity of fishes: biology, evolution, and ecology*, *2nd edn*. Chichester: Wiley-Blackwell.

Horn MH, Correa SB, Parolin P, Pollux BJA, Anderson JT, Lucas C, Widmann P, Albertus T, Galetti M, Goulding M. 2011. Seed dispersal by fishes in tropical and temperate fresh waters: The growing evidence. *Acta Oecologica* **37:** 561–577.

Ives AR, Midford PE, Garland T Jr. 2007. Within-species variation and measurement error in phylogenetic comparative methods. *Systematic Biology* **56:** 252–270.

Jégu M, Dos Santos GM. 2002. Révision du statut de Myleus setiger Müller & Troschel, 1844 et de Myleus knerii (Steindachner, 1881) (Teleostei: Characidae: Serrasalminae) avec une description complémentaire des deux espèces. *Cybium* **26:** 33–57.

Jégu M, Dos Santos GM, Keith P, Le Bail P-Y. 2002a. Description complémentaire et réhabilitation de *Tometes trilobatus* Valenciennes, 1850, espèce-type de Tometes Valenciennes (Characidae: Serrasalminae). *Cybium* **26:** 99–122.

Jégu M, Keith P. 2005. Threatened fishes of the world: *Tometes lebaili* (Jégu, Keith, & Belmont-Jégu 2002) (Characidae: Serrasalminae). *Environmental Biology of Fishes* **72:** 378.

Jégu M, Keith P, Belmont-Jégu E. 2002b. Une nouvelle espèce de *Tometes* (Teleostei : Characidae : Serrasalminae) du bouclier guyanais, *Tometes lebaili* N. Sp. *Bulletin Français de la Pêche et de la Pisciculture* **364:** 23–48.

Downloaded from https://academic.oup.com/biolinnean/advance-article-abstract/doi/10.1093/biolinnean/bly092/5057832
by Natural History Museum user
on 24 July 2018

Lauder GV. 1981. Intraspecific functional repertoires in the feeding mechanism of the characoid fishes *Lebiasina*, *Hoplias* and *Chalceus*. *Copeia* 1981: 154.

Ladich F. 1999. Did auditory sensitivity and vocalization evolve independently in otophysan fishes? *Brain, Behavior and Evolution* **53:** 288–304.

Leite RG, Jégu M. 1990. Régime alimentaire de deux espèces d'*Acnodon* (Characiformes, Serrasalmidae) et habitudes lepidophages de *A. normani*. *Cybium* **14:** 353–359.

Lugli M, Fine ML. 2003. Acoustic communication in two freshwater gobies: ambient noise and short-range propagation in shallow streams. *The Journal of the Acoustical Society of America* **114:** 512–521.

Lugli M, Fine ML. 2007. Stream ambient noise, spectrum and propagation of sounds in the goby *Padogobius martensii*: sound pressure and particle velocity. *The Journal of the Acoustical Society of America* **122:** 2881–2892.

Lychakov DV, Rebane YT. 2000. Otolith regularities. *Hearing Research* **143:** 83–102.

Machado-Allison A, Garcia C. 1986. Food habits and morphological changes during ontogeny in three serrasalmin fish species of the Venezuelan floodplains. *Copeia* **1986:** 193–195.

Markl H. 1972. Aggression and prey capture in piranhas (Serrasalminae, Characidae). *Zeitschrift fur Tierpsychologie* **30:** 190–216.

Mélotte G, Parmentier E, Michel C, Herrel A, Boyle K. 2018. Hearing capacities and morphology of the auditory system in Serrasalmidae (Teleostei: Otophysi). *Scientific Reports* **8:** 1281.

Mirande JM. 2009. Weighted parsimony phylogeny of the family Characidae (Teleostei: Characiformes). *Cladistics* **25:** 574–613.

Mitteroecker P, Bookstein F. 2011. Linear discrimination, ordination, and the visualization of selection gradients in modern morphometrics. *Evolutionary Biology* **38:** 100–114.

Mol JH. 2006. Attacks on humans by the piranha *Serrasalmus rhombeus* in Suriname. *Studies on Neotropical Fauna and Environment* **41:** 189–195.

Nelson EM. 1961. The swim bladder in the Serrasalminae with notes on additional morphological features. *Fieldiana Zoology* **56:** 603–624.

Nico LG. 1991. *Trophic ecology of piranhas (Characidae: Serrasalminae) from savanna and forest regions in the Orinoco River basin of Venezuela*. PhD thesis. University of Florida, Gainesville.

Nico LG, Taphorn DC. 1988. Food habits of piranhas in the low Llanos of Venezuela. *Biotropica* **20:** 311–321.

Nilsson PA, Brönmark C. 2000. Prey vulnerability to a gape-size limited predator: behavioural and morphological impacts on northern pike piscivory. *Oikos* **88:** 539–546.

Ortí G, Sivasundar A, Dietz K, Jégu M. 2008. Phylogeny of the Serrasalmidae (Characiformes) based on mitochondrial DNA sequencyes. *Genetics and Molecular Biology* **31:** 343–351.

Paradis E, Claude J, Strimmer K. 2004. APE: Analyses of phylogenetics and evolution in R language. *Bioinformatics* **20:** 289–290.

Parmentier E, Mann K, Mann D. 2011. Hearing and morphological specializations of the mojarra (Eucinostomus argenteus). *The Journal of Experimental Biology* **214:** 2697–2701.

Parolin P, Waldhoff D, Piedade MTF. 2010. Fruit and seed chemistry, biomass and dispersal. In: Junk W, Piedade M, Wittmann F, Schöngart J, Parolin P, eds. *Amazonian floodplain forests. Ecological studies (analysis and synthesis), Vol. 210.* Dordecht: Springer, Dordrecht, 243–258.

Piedade MT, Parolin P, Junk WJ. 2006. Phenology, fruit production and seed dispersal of *Astrocaryum jauari* (Arecaceae) in Amazonian black water floodplains. *Revista de Biologia Tropical* **54:** 1171–1178.

Pistore AE, Barry TN, Bowles E, Sharma R, Vanderzwan SL, Rogers SM, Jamniczky HA. 2016. Characterizing phenotypic divergence using three-dimensional geometric morphometrics in four populations of threespine stickleback (*Gasterosteus aculeatus*; Pisces: Gasterosteidae) in Katmai National Park and Preserve, Alaska. *Canadian Journal of Zoology* **94:** 463–472.

Popper AN. 1972. Pure-tone auditory thresholds for the carp, *Cyprinis carpio*. *Journal of the Acoustical Society of America* **52:** 1714–1717.

Popper AN, Fay RR. 1973. Sound detection and processing by teleost fishes: a critical review. *The Journal of the Acoustical Society of America* **53:** 1515–1529.

Popper AN, Fay RR. 2011. Rethinking sound detection by fishes. *Hearing Research* **273:** 25–36.

Popper AN, Platt C. 1993. Inner ear and lateral line. In: Evans DH, ed. *The physiology of fishes*. Boca Raton: CRC Press, 99–136.

Popper AN, Ramcharitar J, Campana SE. 2005. Why otoliths? Insights from inner ear physiology and fisheries biology. *Marine and Freshwater Research* **56:** 497–504.

R Core Team. 2017. *R:A language and environment for statistical computing.* Vienna: R Foundation for Statistical Computing. Available at http://www.R-project.org (accessed 14 July 2018).

Revell LJ. 2012. phytools: an R package for phylogenetic comparative biology (and other things). *Methods in Ecology and Evolution* **3:** 217–223.

Revell LJ. 2017. *Phylogenetic tools for comparative biology (and other things). R package version on 0.6–20*. Available at https://cran.r-project.org/web/packages/phytools/index.html (accessed 14 July 2018).

Rohlf FJ, Slice D. 1990. Extensions of the Procrustes method for the optimal superimposition of landmarks. *Systematic Zoology* **39:** 40–59.

Sallan LC, Friedman M. 2012. Heads or tails: staged diversification in vertebrate evolutionary radiations. *Proceedings of the Royal Society B: Biological Sciences* **279:** 2025–2032.

Sanderson MJ, Purvis A, Henze C. 1998. Phylogenetic supertrees: assembling the trees of life. *Trends in Ecology & Evolution* **13:** 105–109.

Sazima I, Machado FA. 1990. Underwater observations of piranhas in western Brazil. *Environmental Biology of Fishes* **28:** 17–31.

Schlager S. 2015. *Morpho: calculations and visualisations related to geometric morphometrics. version 2.3.0*. Available at https://cran.r-project.org/package=Morpho

Schmitz L, Wainwright PC. 2011a. Nocturnality constrains morphological and functional diversity in the eyes of reef fishes. *BMC Evolutionary Biology* **11:** 338.

Schmitz L, Wainwright PC. 2011b. Ecomorphology of the eyes and skull in zooplanktivorous labrid fishes. *Coral Reefs* **30:** 415–428.

Downloaded from https://academic.oup.com/biolinnean/advance-article-abstract/doi/10.1093/biolinnean/bly092/5057832
by Natural History Museum user
on 24 July 2018

Segall M, Cornette R, Fabre AC, Godoy-Diana R, Herrel A. 2016. Does aquatic foraging impact head shape evolution in snakes? *Proceedings of the Royal Society B: Biological Sciences* **283:** 20161645.

Sidlauskas B. 2008. Continuous and arrested morphological diversification in sister clades of characiform fishes: a phylomorphospace approach. *Evolution* **62:** 3135–3156.

Stabentheiner A. 1988. Correlations between hearing and sound production in piranhas. *Journal of Comparative Physiology A* **162:** 67–76.

Stayton CT. 2017. *convevol: quantifies and assesses the significance of convergent evolution. R package version 1.1*. Available at https://cran.r-project.org/package=convevol/index.html (accessed 14 July 2018).

Striedter GF, Northcutt RG. 2006. Head size constrains forebrain development and evolution in ray-finned fishes. *Evolution & Development* **8:** 215–222.

Thompson AW, Betancur-R R, López-Fernández H, Ortí G. 2014. A time-calibrated, multi-locus phylogeny of piranhas and pacus (Characiformes: Serrasalmidae) and a comparison of species tree methods. *Molecular Phylogenetics and Evolution* **81:** 242–257.

Tonolla D, Lorang MS, Heutschi K, Gotschalk CC, Tockner K. 2011. Characterization of spatial heterogeneity in underwater soundscapes at the river segment scale. *Limnology and Oceanography* **56:** 2319–2333.

Tricas TC, Boyle KS. 2015. Sound pressure enhances the hearing sensitivity of Chaetodon butterflyfishes on noisy coral reefs. *The Journal of Experimental Biology* **218:** 1585–1595.

Ward AB, Brainerd EL. 2007. Evolution of axial patterning in elongate fishes. *Biological Journal of the Linnean Society* **90:** 97–116.

Webb PW. 1984. Form and function in fish swimming. *Scientific American* **251:** 72–83.

Webb PW. 2005. Stability and maneuverablility. In: Shadwick RE, Lauder GV, eds. *Fish biomechanics*. San Diego: Academic Press, 281–332.

Weber EH. 1820. *De aure et auditu hominis et animalium. Pars I. de aure animalium aquatilium*. Leipzig: Gerhard Fleischer.

Wiley DF, Amenta N, Alcantara DA, Ghosh D, Kil YJ, Delson E, Harcourt-Smith W, Rohlf FJ, St John K, Hammann B. 2005. Evolutionary morphing. *Proceedings of the IEEE Visualization 2005 (VIS'05)*. Minneapolis: IEEE, 431–438.

Winterbottom R. 1974. A descriptive synonymy of the striated muscles of the Teleostei. *Proceedings of the Academy of Natural Sciences of Philadelphia* **125:** 225–317.

Yan HY, Fine ML, Horn NS, Colón WE. 2000. Variability in the role of the gasbladder in fish audition. *Journal of Comparative Physiology. A, Sensory, Neural, and Behavioral Physiology* **186:** 435–445.

Zuanon JAS. 1999. *História natural da ictiofauna de corredeiras do rio Xingu, na região de Altamira, Pará.* PhD. Thesis, Universidade Estadual de Campinas, Campinas.

SUPPORTING INFORMATION

Additional Supporting Information may be found in the online version of this article at the publisher's web-site.

Table S1. Details of the specimens used in study.

Figure S1. Phylogenetic hypothesis of serrasalmid species used in our study. Composite tree constructed from Ortí *et al.* (2008), Thompson *et al.* (2014) and Andrade *et al.* (2017). Branch length data are in millions of years (ma). Ecological groups of each species are indicated on the right. Nodes 1, 2 and 3 indicate the 'pacu clade', '*Myleus*-pacus clade' and 'piranha clade', respectively (*sensu* Ortí *et al.*, 2008; Thompson *et al.* 2014).

Figure S2. Superimposed landmarks (LMs) of *Catoprion mento* (red LMs), the mean shape of several *Myleus*-pacus (*Myleus asterias*, *Myloplus rubripinnis*, *Mylesinus schomburgkii*; purple LMs), and the mean shape of all 20 serrasalmid species in the study (orange LMs). Mean LM positions were calculated using the 'mshape' function of the R package 'geomorph' (Adams *et al.*, 2016). *Catoprion mento* LMs are the mean of individuals and the other means (several *Myleus*-pacus, and the dataset grand mean) are means of species means. Superimposed LMs were generated with the 'deformGrid3d' function in the R package 'Morpho' (Schlager, 2015). *Catoprion mento* vs. the mean shape of several *Myleus*-pacus (A, D, G, J, M), *Catoprion mento* vs. the mean shape of all serrasalmids in the study (B, E, H, K, N), and the mean shape of several *Myleus*-pacus vs. the mean shape of all serrasalmids in the study (C, F, I, L, O). Lateral view (A–C), dorsal view (D–F), ventral view (G–I), caudal view (J–L) and frontal view (M–O).

Figure S3. Superimposed landmarks (LMs) of *Mylossoma* (black LMs), *Metynnis* (grey LMs), and the mean shape of all 20 serrasalmid species in the study (orange LMs). Mean LM positions were calculated using the 'mshape' function of the R package 'geomorph' (Adams *et al.*, 2016). *Mylossoma* LMs are the mean of species means (*M. aureum* and *M. duriventre*), *Metynnis* LMs are the mean of species means (*M. hypsauchen* and *M. lippincottianus*), and the dataset grand mean is the mean of all 20 species means in the study. Superimposed LMs were generated with the 'deformGrid3d' function in the R package 'Morpho' (Schlager, 2015). *Mylossoma* vs. *Metynnis* (A, D, G, J, M), *Mylossoma* vs. the mean shape of all serrasalmids in the study (B, E, H, K, N), and *Metynnis* vs. the mean shape of all serrasalmids in the study (C, F, I, L, O). Lateral view (A–C), dorsal view (D–F), ventral view (G–I), caudal view (J–L) and frontal view (M–O).

Figure S4. Relationship between centroid size (ln centroid size) and shape (PC1) for the otic neurocranium. Carnivores are shown in red, rheophilic herbivores in blue and frugivore/granivores in green.

Downloaded from https://academic.oup.com/biolinnean/advance-article-abstract/doi/10.1093/biolinnean/bly092/5057832
by Natural History Museum user
on 24 July 2018